Bio fluid mechanics – blood circulation

supplementary material / lecture notes

Timo Koch and Martin Schneider

January 2023

These lecture notes are being updated from time to time and sections may be added or deleted upon request. We try our best but cannot guarantee that all content is indeed correct. In case you find errors in the script, please report them at `timokoch@uio.no` so we can fix them.

1 Cylinder coordinate system

Since blood vessels can often be described as tubes with circular cross-sections, describing the governing equations in a (local) cylinder coordinate system is often convenient and yields simpler expressions. In the following, we assume that the main cylinder axis is aligned with the z-axis of a corresponding Cartesian coordinate system. Under this assumption, we can define the following coordinate transformations in terms of the Cartesian coordinates (x, y, z):

$$x = r\cos(\theta), \quad y = r\sin(\theta), \quad z = z, \tag{1}$$

where r is the radial coordinate, θ the circumferential coordinate, and z the axial coordinate. An arbitrary vector field, $\boldsymbol{u} : \mathbb{R}^3 \to \mathbb{R}^3$, can be expressed in the cylinder coordinates (r, θ, z) by

$$\boldsymbol{u} = u_r \boldsymbol{e}_r + u_\theta \boldsymbol{e}_\theta + u_z \boldsymbol{e}_z. \tag{2}$$

with the basis vectors $\boldsymbol{e}_r = (\cos(\theta), \sin(\theta), 0)^T$, $\boldsymbol{e}_\theta = (-\sin(\theta), \cos(\theta), 0)^T$, $\boldsymbol{e}_z = (0, 0, 1)^T$.

Differential operators can be expressed in cylinder coordinates as well and have slightly different representations than in Cartesian coordinates. For the gradient of a scalar field, $u : \mathbb{R}^3 \to \mathbb{R}$, we get

$$\operatorname{grad}(u) \equiv \nabla u = \frac{\partial u}{\partial r}\boldsymbol{e}_r + \frac{1}{r}\frac{\partial u}{\partial \theta}\boldsymbol{e}_\theta + \frac{\partial u}{\partial z}\boldsymbol{e}_z. \tag{3}$$

For the divergence of a vector field $\boldsymbol{u} : \mathbb{R}^3 \to \mathbb{R}^3$, we get

$$\operatorname{div}(\boldsymbol{u}) \equiv \nabla \cdot \boldsymbol{u} = \frac{1}{r}\frac{\partial (r u_r)}{\partial r} + \frac{1}{r}\frac{\partial u_\theta}{\partial \theta} + \frac{\partial u_z}{\partial z}. \tag{4}$$

For the curl of a vector field $\boldsymbol{u}$, we get

$$\operatorname{curl}(\boldsymbol{u}) \equiv \nabla \times \boldsymbol{u} = \left(\frac{1}{r}\frac{\partial u_z}{\partial \theta} - \frac{\partial u_\theta}{\partial z}\right)\boldsymbol{e}_r + \left(\frac{\partial u_r}{\partial z} - \frac{\partial u_z}{\partial r}\right)\boldsymbol{e}_\theta + \left(\frac{1}{r}\frac{\partial (r u_\theta)}{\partial r} - \frac{1}{r}\frac{\partial u_r}{\partial \theta}\right)\boldsymbol{e}_z. \tag{5}$$

For the Laplace operator applied to a scalar field u, we get

$$\operatorname{div}\operatorname{grad}(u) \equiv \nabla^2 u \equiv \Delta u = \frac{1}{r}\frac{\partial}{\partial r}\left(r\frac{\partial u}{\partial r}\right) + \frac{1}{r^2}\frac{\partial^2 u}{\partial \theta^2} + \frac{\partial^2 u}{\partial z^2}. \tag{6}$$

For the Laplace operator applied to a vector field $\boldsymbol{u}$, we get

$$\nabla^2 \boldsymbol{u} \equiv \Delta \boldsymbol{u} = \left(\Delta u_r - \frac{u_r}{r^2} - \frac{2}{r^2}\frac{\partial u_\theta}{\partial \theta}\right)\boldsymbol{e}_r + \left(\Delta u_\theta - \frac{u_\theta}{r^2} - \frac{2}{r^2}\frac{\partial u_r}{\partial \theta}\right)\boldsymbol{e}_\theta + \Delta u_z \boldsymbol{e}_z, \tag{7}$$

where we reused the scalar Laplace operator for the sake of brevity.

The integration elements are also transformed. The volume element $\mathrm{d}V$ is given by $\mathrm{d}V = r\,\mathrm{d}r\mathrm{d}\theta\mathrm{d}z$. The area element $\mathrm{d}A$ is given by $\mathrm{d}A = r\,\mathrm{d}r\mathrm{d}\theta$. As an example, a volume integral over a cylinder with radius R and length L and integrand (integral kernel) 1 yields the cylinder volume,

$$\int_V 1\,\mathrm{d}V = \int_0^L \int_0^{2\pi} \int_0^R 1\; r\,\mathrm{d}r\mathrm{d}\theta\mathrm{d}z = \int_0^L \int_0^{2\pi} \frac{1}{2}R^2\mathrm{d}\theta\mathrm{d}z = \int_0^L \pi R^2\mathrm{d}z = \pi R^2 L. \tag{8}$$

2 Stress tensor

For incompressible Newtonian fluids, the deviatoric[1] stress tensor $\boldsymbol{\tau}$ (in Cartesian coordinates) is given by

$$\boldsymbol{\tau} = \begin{bmatrix} \tau_{xx} & \tau_{xy} & \tau_{xz} \\ \tau_{yx} & \tau_{yy} & \tau_{yz} \\ \tau_{zx} & \tau_{zy} & \tau_{zz} \end{bmatrix} = \mu \begin{bmatrix} 2\frac{\partial v_x}{\partial x} & \frac{\partial v_x}{\partial y} + \frac{\partial v_y}{\partial x} & \frac{\partial v_x}{\partial z} + \frac{\partial v_z}{\partial x} \\ \frac{\partial v_x}{\partial y} + \frac{\partial v_y}{\partial x} & 2\frac{\partial v_y}{\partial y} & \frac{\partial v_y}{\partial z} + \frac{\partial v_z}{\partial y} \\ \frac{\partial v_x}{\partial z} + \frac{\partial v_z}{\partial x} & \frac{\partial v_y}{\partial z} + \frac{\partial v_z}{\partial y} & 2\frac{\partial v_z}{\partial z} \end{bmatrix} = \mu\left(\nabla\boldsymbol{v} + (\nabla\boldsymbol{v})^T\right) = 2\mu\boldsymbol{D}, \tag{9}$$

where the off-diagonal entries τ_{ij} are called shear stresses and the diagonal elements τ_{ii} normal stresses, $\boldsymbol{v} = (v_x, v_y, v_z)^T$ denotes the velocity vector, μ the dynamic viscosity, $\nabla\boldsymbol{u}$, the gradient of vector $\boldsymbol{u}$, A^T the transpose of matrix A, and $\boldsymbol{D}$ is the rate-of-strain tensor.

The deviatoric stress tensor appears in the general momentum balance as part of the Cauchy stress tensor (or true stress tensor) $\boldsymbol{\sigma}$ which can be decomposed into a deviatoric and a non-deviatoric part. For incompressible Newtoninan fluids, we have

$$\boldsymbol{\sigma} = \boldsymbol{\tau} - p\boldsymbol{I} = 2\mu\boldsymbol{D} - p\boldsymbol{I}, \tag{10}$$

where p is the hydrostatic fluid pressure and $\boldsymbol{I}$ is the identity matrix (second-order tensor with 1 as diagonal elements and all other elements zero).

2.1 Generalized Newtonian fluids

The constitutive equation for an incompressible Newtonian fluid is given by Eq. (9). We will now define the shear rate magnitude $\dot{\gamma}$ as

$$\dot{\gamma} := \sqrt{2\boldsymbol{D} : \boldsymbol{D}} \equiv \sqrt{2D_{ij}D_{ij}}. \tag{11}$$

Using this definition, constitutive models for so-called generalized Newtonian fluids can be formulated, that is models of the form

$$\boldsymbol{\tau} = 2\mu(\dot{\gamma})\boldsymbol{D}, \tag{12}$$

where μ is the viscosity function that depends on the shear rate. One example is the generalized power law, where

$$\mu(\dot{\gamma}) := \lambda(\dot{\gamma})\dot{\gamma}^{n(\dot{\gamma})-1}, \tag{13}$$

and the parameters λ and n that may also depend on $\dot{\gamma}$ have to be determined experimentally for a given fluid. An overview of different functions that have been proposed to describe generalized Newtonian fluids is, for instance, given by Irgens [6]. Blood (as well as many other colloid systems and suspensions) can be described as a shear-thinning fluid, that is the apparent viscosity μ decreases with increasing shear rate. (In contrast, the apparent viscosity of a shear-thickening fluid increases with increasing shear rate.)

3 Incompressible Navier-Stokes equations

The motion of incompressible fluids is governed by the (incompressible) Navier-Stokes equations,

$$\rho\frac{\partial\boldsymbol{v}}{\partial t} + \nabla\cdot(\rho\boldsymbol{v}\otimes\boldsymbol{v} - \boldsymbol{\sigma}) - \rho\boldsymbol{b} = \boldsymbol{0}, \tag{14a}$$

$$\nabla\cdot\boldsymbol{v} = 0, \tag{14b}$$

[1] A *deviator* or *deviatoric* tensor is a second order tensor A with zero trace, $\mathrm{tr}(A) = \sum_{i=0}^{n} a_{ii} = 0$. This property can be easily verified for the given $\boldsymbol{\tau}$ by employing the mass balance equation for incompressible fluids, $\nabla\cdot\boldsymbol{v} = \mathrm{tr}(\boldsymbol{D}) = 0$.

where $\otimes$ denotes the outer vector product (yielding a second-order tensor), and $\boldsymbol{b}$ is a body force (e.g. gravity). The first equation is also called the balance of momentum, while the second equation is the balance of mass. The mass balance for an incompressible fluid is also sometimes referred to as the *incompressibility constraint* and states that the velocity field is divergence-free.

For blood flow modeling it is most convenient to write the incompressible Navier-Stokes equations in cylindrical coordinates:

$$\frac{\partial v_r}{\partial t} + v_r\frac{\partial v_r}{\partial r} + \frac{v_\theta}{r}\frac{\partial v_r}{\partial \theta} + v_z\frac{\partial v_r}{\partial z} - \frac{v_\theta^2}{r} + \frac{1}{\rho}\frac{\partial p}{\partial r} - \frac{\mu}{\rho}\left(\frac{1}{r}\frac{\partial}{\partial r}\left(r\frac{\partial v_r}{\partial r}\right) + \frac{1}{r^2}\frac{\partial^2 v_r}{\partial \theta^2} + \frac{\partial^2 v_r}{\partial z^2} - \frac{v_r}{r^2} - \frac{2}{r^2}\frac{\partial v_\theta}{\partial \theta}\right) - b_r = 0, \quad (15)$$

$$\frac{\partial v_\theta}{\partial t} + v_r\frac{\partial v_\theta}{\partial r} + \frac{v_\theta}{r}\frac{\partial v_\theta}{\partial \theta} + v_z\frac{\partial v_\theta}{\partial z} - \frac{v_r v_\theta}{r} + \frac{1}{\rho}\frac{\partial p}{\partial r} - \frac{\mu}{\rho}\left(\frac{1}{r}\frac{\partial}{\partial r}\left(r\frac{\partial v_\theta}{\partial r}\right) + \frac{1}{r^2}\frac{\partial^2 v_\theta}{\partial \theta^2} + \frac{\partial^2 v_\theta}{\partial z^2} - \frac{v_\theta}{r^2} + \frac{2}{r^2}\frac{\partial v_r}{\partial \theta}\right) - b_\theta = 0, \quad (16)$$

$$\frac{\partial v_z}{\partial t} + v_r\frac{\partial v_z}{\partial r} + \frac{v_\theta}{r}\frac{\partial v_z}{\partial \theta} + v_z\frac{\partial v_z}{\partial z} + \frac{1}{\rho}\frac{\partial p}{\partial z} - \frac{\mu}{\rho}\left(\frac{1}{r}\frac{\partial}{\partial r}\left(r\frac{\partial v_z}{\partial r}\right) + \frac{1}{r^2}\frac{\partial^2 v_z}{\partial \theta^2} + \frac{\partial^2 v_z}{\partial z^2}\right) - b_z = 0, \quad (17)$$

$$\frac{1}{r}\frac{\partial (r v_r)}{\partial r} + \frac{1}{r}\frac{\partial v_\theta}{\partial \theta} + \frac{\partial v_z}{\partial z} = 0. \quad (18)$$

4 Blood flow models

4.1 Fully developed flow in rigid vessels

We start with the incompressible Navier-Stokes for a Newtonian fluid in cylindrical coordinates, neglect external body forces (gravity), and assume $v_\theta = 0$, $\partial_\theta(\cdot) = 0$ (circumferential velocity component and derivatives), leaving us with two momentum balances for radial and axial velocity components v_r and v_z and a volume balance equation (dividing the mass balance equation by the density ρ),

$$\frac{\partial v_r}{\partial t} + v_r\frac{\partial v_r}{\partial r} + v_z\frac{\partial v_r}{\partial z} + \frac{1}{\rho}\frac{\partial p}{\partial r} - \frac{\mu}{\rho}\left(\frac{1}{r}\frac{\partial}{\partial r}\left(r\frac{\partial v_r}{\partial r}\right) + \frac{\partial^2 v_r}{\partial z^2} - \frac{v_r}{r^2}\right) = 0, \quad (19)$$

$$\frac{\partial v_z}{\partial t} + v_r\frac{\partial v_z}{\partial r} + v_z\frac{\partial v_z}{\partial z} + \frac{1}{\rho}\frac{\partial p}{\partial z} - \frac{\mu}{\rho}\left(\frac{1}{r}\frac{\partial}{\partial r}\left(r\frac{\partial v_z}{\partial r}\right) + \frac{\partial^2 v_z}{\partial z^2}\right) = 0, \quad (20)$$

$$\frac{1}{r}\frac{\partial (r v_r)}{\partial r} + \frac{\partial v_z}{\partial z} = 0. \quad (21)$$

For fully developed flow and rigid vessel walls, we make the additional assumption that the radial velocity component vanishes,

$$\frac{\partial p}{\partial r} = 0, \quad (22)$$

$$\frac{\partial v_z}{\partial t} + v_z\frac{\partial v_z}{\partial z} + \frac{1}{\rho}\frac{\partial p}{\partial z} - \frac{\mu}{\rho}\left(\frac{1}{r}\frac{\partial}{\partial r}\left(r\frac{\partial v_z}{\partial r}\right) + \frac{\partial^2 v_z}{\partial z^2}\right) = 0, \quad (23)$$

$$\frac{\partial v_z}{\partial z} = 0, \quad (24)$$

and the combination of the latter two equations yields

$$\frac{\partial v_z}{\partial t} + \frac{1}{\rho}\frac{\partial p}{\partial z} - \frac{\mu}{\rho}\left(\frac{1}{r}\frac{\partial}{\partial r}\left(r\frac{\partial v_z}{\partial r}\right)\right) = 0, \quad (25)$$

where the pressure is independent of r.

4.2 Fully developed steady flow in rigid vessels

One of the best-known simplifications for the incompressible Navier-Stokes equations describes the steady flow in a rigid straight circular pipe. Since we will look at the steady-state solution (for instance given assuming a steady pressure difference between the inlet and the outlet of a straight pipe section), time derivatives vanish. Therefore, Eq. (25) becomes

$$\frac{1}{r}\frac{\partial}{\partial r}\left(r\frac{\partial v_z}{\partial r}\right) = \frac{1}{\mu}\frac{\partial p}{\partial z}. \tag{26}$$

Recalling that the pressure is only a function of z, we can solve for v_z by integrating twice

$$\int \frac{\partial}{\partial r}\left(r\frac{\partial v_z}{\partial r}\right)\mathrm{d}r = \int \frac{1}{\mu}\frac{\partial p}{\partial z} r \mathrm{d}r, \tag{27}$$

$$r\frac{\partial v_z}{\partial r} = \frac{1}{2\mu}\frac{\partial p}{\partial z} r^2 + C_1, \tag{28}$$

for $r = 0$, we get $C_1 = 0$, thus

$$\frac{\partial v_z}{\partial r} = \frac{1}{2\mu}\frac{\partial p}{\partial z} r, \tag{29}$$

$$v_z = \frac{1}{4\mu}\frac{\partial p}{\partial z} r^2 + C_2, \tag{30}$$

and the constant C_2 is determined by assuming a no-slip boundary condition at $r = R$, i.e. $v_z(R) = 0$, yields

$$C_2 = -\frac{1}{4\mu}\frac{\partial p}{\partial z} R^2 \quad \Rightarrow \quad v_z(r) = -\frac{R^2}{4\mu}\frac{\partial p}{\partial z}\left[1 - \left(\frac{r}{R}\right)^2\right]. \tag{31}$$

The average velocity found by integration over a cross-section

$$\overline{v_z} = -\frac{1}{\pi R^2}\frac{1}{4\mu}\frac{\partial p}{\partial z}\int_0^{2\pi}\int_0^{R}\left[1 - \left(\frac{r}{R}\right)^2\right] r \mathrm{d}r\mathrm{d}\theta = -\frac{1}{2\mu}\frac{\partial p}{\partial z}\left[\frac{1}{2}r^2 - \frac{1}{4}\frac{r^4}{R^2}\right]_0^R \tag{32}$$

$$= -\frac{R^2}{8\mu}\frac{\partial p}{\partial z} = \frac{1}{2}v_z(0) := \frac{1}{2}v_{\max}, \tag{33}$$

and the flow rate Q is given by $Q = A\overline{v_z} = \pi R^2 \overline{v_z}$, for a circular cross-section, which gives the well-known Hagen-Poiseuille law, relating flow rate and pressure gradient in a straight tube

$$Q = -\frac{\pi R^4}{8\mu}\frac{\partial p}{\partial z}. \tag{34}$$

4.3 Fully developed pulsatile flow in rigid vessels

In this section, we analyze pulsatile pipe flow in a rigid vessel, explain how the Womersley number appears in the dimensional analysis of the governing equations, and derive Womersley's well-known analytical solution for velocity profiles when the flow is driven by oscillating pressure gradients. We start with equation Eq. (25) from the previous section. This time, we are interested in how the velocity profile evolves with time and therefore cannot neglect the time derivative in Eq. (25).

We can arrive at a non-dimensional form of Eq. (25) by introducing the dimensionless quantities $z^* = z/R$, $t^* = t\omega$, $v_z^* = v_z/V$, $p^* = pR/(\mu V)$, where R (m) is a characteristic length scale (here we choose a characteristic vessel radius), ω is a characteristic angular frequency (s^{-1}), and V ($\mathrm{m\,s}^{-1}$) is a characteristic velocity of the system,

$$\mathrm{Wo}^2\frac{\partial v_z^*}{\partial t^*} + \frac{\partial p^*}{\partial z^*} - \frac{1}{r^*}\frac{\partial}{\partial r^*}\left(r^*\frac{\partial v_z^*}{\partial r^*}\right) = 0, \tag{35}$$

where we introduced the Womersley number $\mathrm{Wo} := R\,(\omega\rho/\mu)^{\frac{1}{2}}$. (Verifying the step from Eq. (25) to Eq. (35) is a good exercise.)

We can now look at the two terms involving v_z^* and see that there are two limit cases. In the case Wo $\gg 1$, Eq. (25) can be reduced to

$$\frac{\partial v_z}{\partial t} + \frac{1}{\rho}\frac{\partial p}{\partial z} = 0, \tag{36}$$

while in the case Wo $\ll 1$, Eq. (25) reduces to

$$\frac{1}{\rho}\frac{\partial p}{\partial z} - \frac{\mu}{\rho}\left(\frac{1}{r}\frac{\partial}{\partial r}\left(r\frac{\partial v_z}{\partial r}\right)\right) = 0. \tag{37}$$

To understand the meaning of the limit cases as well as the case of moderate Womersley numbers, Eq. (35), we will choose a harmonic periodically oscillating pressure gradient

$$\frac{\partial p}{\partial z} = P' e^{i\omega t} = P'\left(\cos\omega t + i\sin\omega t\right) \tag{38}$$

where P' is the magnitude of the axial pressure gradient, and therefore look for a harmonic velocity solution of the form

$$v_z(r,t) = V_z(r)e^{i\omega t} = V_z(r)\left(\cos\omega t + i\sin\omega t\right). \tag{39}$$

Inserting these functions into the equations and taking their real part will give us a solution for the velocity profile corresponding to this oscillating pressure gradient. Note that although we look at a profile with a single frequency $f = \omega/(2\pi)$, we can construct arbitrary periodic solutions by superposition since Eq. (25) is linear in v_z and p.

4.3.1 The case Wo $\gg 1$

Inserting Eqs. (38) and (39) into Eq. (36) yields

$$V_z = -\frac{1}{\rho\omega i}P', \quad \Rightarrow v_z(t) = -\frac{1}{\rho\omega i}P'e^{i\omega t}, \tag{40}$$

and taking the real parts of the velocity profile and the pressure gradient yields

$$\Re(v_z(t)) = -\frac{1}{\rho\omega}P'\sin\omega t, \quad \Re\left(\frac{\partial p}{\partial z}\right) = P'\cos\omega t. \tag{41}$$

For this simple configuration, we could have directly started with the real part of the pressure gradient without difficulty. However, we use complex numbers here to prepare for the more general case below where separating real and imaginary part would lead to a much more cumbersome representation of the solution. This means the velocity does not depend on the radial position (plug flow profile) and its phase is shifted by 90° with respect to the pressure gradient. This flow configuration can be characterized as fully inertia-dominated.

4.3.2 The case Wo $\ll 1$

Inserting Eqs. (38) and (39) into Eq. (37) multiplying with r and dividing by μ yields

$$\frac{1}{\mu}P'r = \frac{\partial}{\partial r}\left(r\frac{\partial V_z}{\partial r}\right) = r\frac{\partial^2 V_z}{\partial r^2} + \frac{\partial V_z}{\partial r}, \tag{42}$$

integrating once (using integration by parts) gives

$$\frac{1}{2\mu}P'r^2 = r\frac{\partial V_z}{\partial r} + C_1, \tag{43}$$

Since the radial derivative of the velocity is zero in the middle of the channel ($r = 0$), $C_1 = 0$. Dividing by r again and integrating once more yields

$$V_z(r) = \frac{1}{4\mu}P'r^2 + C_2, \tag{44}$$

and finally by using a no-slip condition on the outer wall ($V_z(r = R) = 0$), we arrive at

$$V_z(r) = -\frac{1}{4\mu}P'(R^2 - r^2), \quad \Rightarrow v_z(r,t) = -\frac{1}{4i\mu}(R^2 - r^2)P'e^{i\omega t}. \tag{45}$$

Taking the real parts of the velocity profile and the pressure gradient yields

$$\Re(v_z(r,t)) = -\frac{1}{4\mu}(R^2 - r^2)P'\cos\omega t, \quad \Re\left(\frac{\partial p}{\partial z}\right) = P'\cos\omega t. \tag{46}$$

This is the well-known Poiseuille flow velocity profile (parabolic profile). Velocity and pressure gradient are 180° out of phase which essentially just means that a negative pressure gradient leads to a positive velocity and vice versa. This flow configuration can be characterised as fully friction dominated, i.e. dominated by viscous forces. Again, we could have worked directly with the real part of the pressure gradient ansatz.

4.3.3 The case of arbitrary Wo

The solution for arbitrary Womersley numbers has been derived by John R. Womersley in [19]. To this end, we insert Eqs. (38) and (39) into Eq. (25),

$$\frac{\mu}{\rho}\left(\frac{1}{r}\frac{\partial}{\partial r}\left(r\frac{\partial V_z}{\partial r}\right)\right) - \omega i V_z = \frac{1}{\rho}P', \tag{47}$$

$$\Rightarrow \frac{\partial^2 V_z}{\partial r^2} + \frac{1}{r}\frac{\partial V_z}{\partial r} + \frac{\rho\omega i^3}{\mu}V_z = \frac{1}{\mu}P', \tag{48}$$

where we used $i^2 = -1$. Equation (48) is linear in V_z, therefore we may seek the solution as a combination of the homogeneous solution and a particular solution. Let us first consider the homogeneous solution, i.e. the solution to

$$\frac{\partial^2 V_z}{\partial r^2} + \frac{1}{r}\frac{\partial V_z}{\partial r} + \frac{\rho\omega i^3}{\mu}V_z = 0. \tag{49}$$

If we multiply Eq. (49) with r^2 and make the substitution $s = r(\rho\omega i^3/\mu)^{\frac{1}{2}}$ (note that $\partial s/\partial r = (\rho\omega i^3/\mu)^{\frac{1}{2}}$),

$$\Rightarrow r^2\frac{\partial^2 V_z}{\partial r^2} + r\frac{\partial V_z}{\partial r} + r^2\frac{\rho\omega i^3}{\mu}V_z = 0, \tag{50}$$

$$\Rightarrow r^2\frac{\partial^2 V_z}{\partial s^2}\left(\frac{\partial s}{\partial r}\right)^2 + r\frac{\partial V_z}{\partial s}\frac{\partial s}{\partial r} + r^2\frac{\rho\omega i^3}{\mu}V_z = 0, \tag{51}$$

$$\Rightarrow s^2\frac{\partial^2 V_z}{\partial s^2} + s\frac{\partial V_z}{\partial s} + s^2 V_z = 0, \tag{52}$$

we obtain Bessel's differential equation (of order zero). Its solution is called Bessel function of the first kind of order zero, denoted by $J_0(s)$, and can be written as the infinite series expansion [1]:

$$J_0(s) = \sum_{m=0}^{\infty}\frac{(-1)^m}{m!m!}\left(\frac{s}{2}\right)^{2m}. \tag{53}$$

Next, we guess a particular solution as $V_z^\diamond = -\frac{1}{\rho\omega i}P'$ and verify that it indeed solves the inhomogeneous equation (48), which is simple since $V_z^\diamond$ is independent of r. Therefore, the full solution may be determined as

$$V_z(r) = CJ_0(s(r)) + V_z^\diamond, \tag{54}$$

with a constant C that can be determined by inserting the no-slip boundary condition on the vessel wall,

$$V_z(R) = 0 = CJ_0(s(R)) - \frac{1}{\rho\omega i}P' \Rightarrow C = \frac{1}{\rho\omega i}P'J_0(s(R))^{-1}. \tag{55}$$

Finally, we obtain the velocity profile $V_z(r)$ and the axial velocity $v_z(r,t)$ as the real part of the complex solution,

$$V_z(r) = -\frac{P'}{\rho\omega i}\left(1 - \frac{J_0(s(r))}{J_0(s(R))}\right), \quad \Re(v_z(r,t)) = \Re\left(-\frac{P'}{\rho\omega i}\left(1 - \frac{J_0(s(r))}{J_0(s(R))}\right)e^{i\omega t}\right), \tag{56}$$

respectively. Substituting s for its expression in terms of r, formulation in terms of the dimensionless radius $r^* = r/R$ and the dimensionless time $t^* = t\omega$, and using the definition of the Womersley number, we obtain

$$\Re(v_z(r^*, t^*)) = \Re\left(-\frac{P'}{\rho\omega i}\left(1 - \frac{J_0(\mathrm{Wo} i^{\frac{3}{2}} r^*)}{J_0(\mathrm{Wo} i^{\frac{3}{2}})}\right) e^{it^*}\right), \quad \Re\left(\frac{\partial p}{\partial z}\right) = P' \cos t^*. \tag{57}$$

The resulting profiles (the well-known Womersley profiles) are plotted in Fig. 1, c.f. [20, Fig.1]. For low Womersley number (Wo = 2), the phase shift between pressure gradient and velocity is 90° and the profile looks parabolic (Poiseuille flow). For intermediate Womersley numbers, it can be observed that the flow is still friction-dominated close to the vessel wall while the flow in the middle of the channel is increasingly dominated by inertial forces. The friction-dominated boundary layer decreases in thickness as the Womersley number increases.

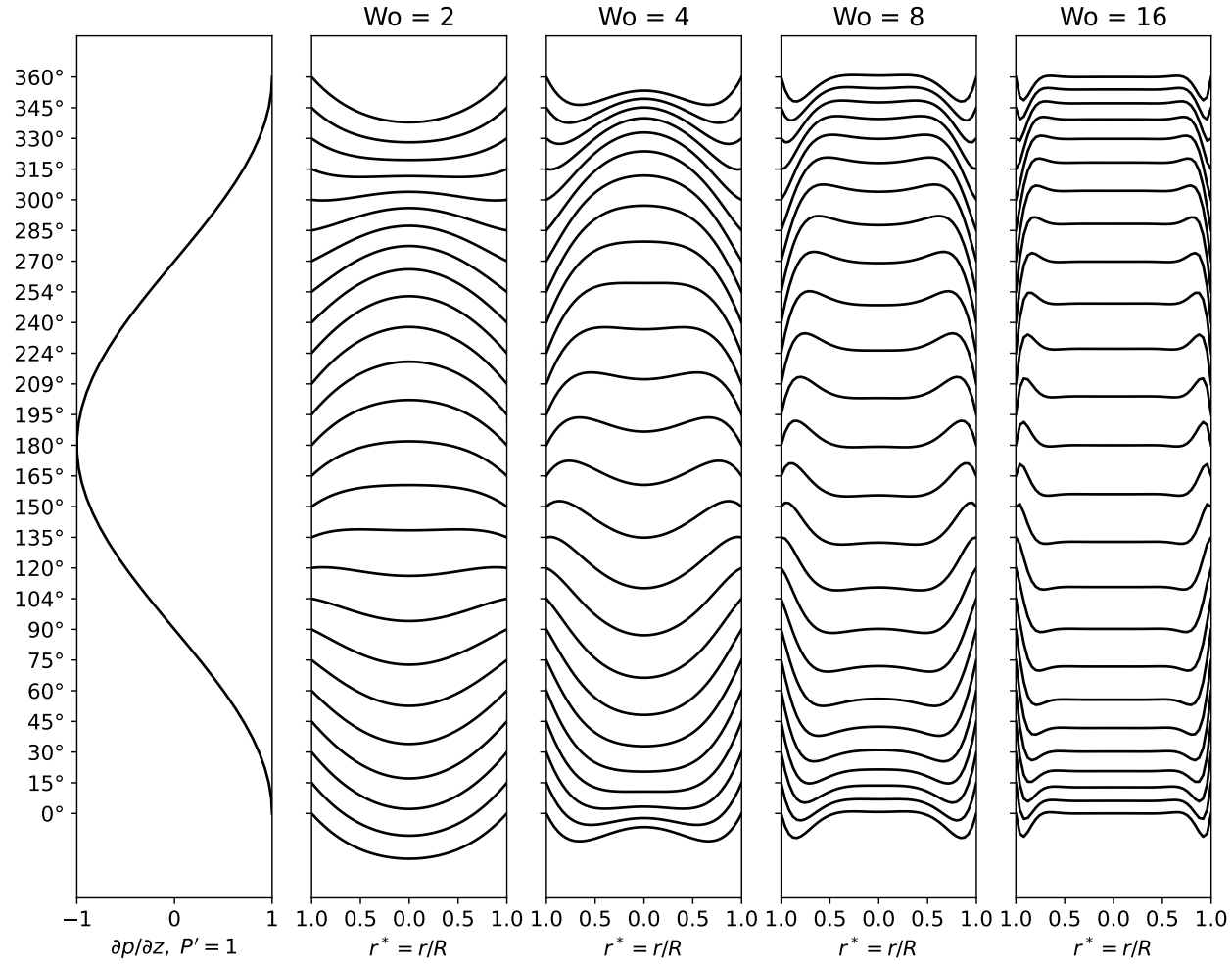

Figure 1: Oscillating pipe flow in a rigid vessel. Velocity profiles overpressure gradient for different Womersley numbers. The figure can be reproduced with the Python script `plot_womersley.py`.

4.4 Pulsatile flow in elastic vessels

Similar solutions than for rigid vessel can also be derived for elastic tube assuming small deformations and a few other restrictions, see e.g. [20]. This might be discussed here in more detail in the future.

4.5 1D models for flow in elastic vessels

In the following, we want to proceed with deriving 1D models for flow in elastic vessels. These models are obtained by reformulating the full Navier-Stokes equations in terms of cross-section averaged quantities using some simplifications. Such models are sometimes called *quasi* 1D models since the modeled geometric domain is still a three-dimensional tube, however the resulting PDEs after model reduction are one-dimensional in space and only dependencies on the axial coordinate appear explicitly. Due to the dimensional reduction of the resulting PDE, the equations can be solved numerically much more efficiently (less discrete degrees of freedom) than fully three-dimension flow models. We will loosely follow the derivations of 1D models presented by Čanić and Kim [21], and Quarteroni and Formaggia [16].

4.5.1 Assumptions

To develop one-dimensional models, we start with several basic assumptions. The system is assumed to be radially symmetric, that is all quantities are independent of the circumferential coordinate. The cross-section $S(z,t)$ of the vessel at axial position z is circular at all times and can be described by

$$A(z,t) = |S(z,t)| = \pi R^2(z,t), \tag{58}$$

where R is the radius function, and by $A = |S|$, we mean that the area A is the measure of the section S. The dominant velocity component in axial direction can be described by

$$v_z(r,z,t) = \bar{v}(z,t)s(r^*), \quad \bar{v} := \frac{1}{A}\int_S v_z \mathrm{d}A \tag{59}$$

where s is the dimensionless velocity profile ($r^* = r/R(z,t)$) and $\bar{v}$ the average cross-sectional velocity. Furthermore, the mean volume flux Q is defined as

$$Q(z,t) := \int_S v_z \mathrm{d}A = A\bar{v}. \tag{60}$$

Displacements only occur radially and we neglect body forces. Finally, the pressure p is assumed to be constant per cross-section. We start the derivation with Eqs. (19) to (21), that is the incompressible Navier-Stokes equations in cylinder coordinates, neglecting the circumferential velocity components and gradients.

4.5.2 Mass balance equation

Under the stated assumptions, the mass balance equation is given by Eq. (21). Integration over the cross-section $S(z,t)$ yields

$$\int_S \frac{1}{r}\frac{\partial(rv_r)}{\partial r}\,\mathrm{d}A + \int_S \frac{\partial v_z}{\partial z}\,\mathrm{d}A = 0. \tag{61}$$

We recall that the area element in cylinder coordinates is $\mathrm{d}A = r\,\mathrm{d}r\mathrm{d}\theta$. Hence, for the first integral we have

$$\int_S \frac{1}{r}\frac{\partial(rv_r)}{\partial r}\,\mathrm{d}A = \int_0^{2\pi}\int_0^R \frac{\partial(rv_r)}{\partial r}\mathrm{d}r\mathrm{d}\theta = 2\pi R \underbrace{v_r(R,t)}_{=\partial R/\partial t} = 2\pi R\frac{\partial R}{\partial t} = \frac{\partial(\pi R^2)}{\partial t} = \frac{\partial A}{\partial t}, \tag{62}$$

where we used the definition of the area, the product rule, and the boundary condition $u_r(R,t) = \partial R/\partial t$, that is the radial fluid velocity component at the vessel wall ($r = R$) is equal to the wall deformation velocity $\dot{R} \equiv \partial R/\partial t$.

For the second term, we apply Leibniz' rule for parameter integrals which is a rule to evaluate integrals with variable bounds and reads for a scalar function $f(z,r,t)$ and variable lower and upper bounds $a(z)$ and $b(z)$,

$$\frac{\mathrm{d}}{\mathrm{d}z}\left(\int_{a(z)}^{b(z)} f(z,r,t)\mathrm{d}r\right) = \int_{a(z)}^{b(z)} \frac{\partial}{\partial z}f(z,r,t)\mathrm{d}r + f(z,b(z),t)\frac{\mathrm{d}}{\mathrm{d}z}b(z) - f(z,a(z),t)\frac{\mathrm{d}}{\mathrm{d}z}a(z). \tag{63}$$

The total derivative of the integral expression is composed of a part where we think of the integration bounds as constants and a second part that evaluates the change due to the change of the integration bounds only. By choosing a function

$$g(z,r,t) := \int_0^{2\pi} v_z r \mathrm{d}\theta = 2\pi v_z r, \tag{64}$$

we can see that in our case the Leibniz rule yields (exchanging terms between right-hand-size and left-hand-side)

$$\begin{aligned}
\int_S \frac{\partial u_z}{\partial z}\,\mathrm{d}A &= \int_0^{R(z)}\int_0^{2\pi} \frac{\partial u_z}{\partial z} r\,\mathrm{d}\theta\mathrm{d}r = \int_0^{R(z)} \frac{\partial}{\partial z}\left(\int_0^{2\pi} u_z r \mathrm{d}\theta\right)\mathrm{d}r = \int_0^{R(z)} \frac{\partial g}{\partial z}\mathrm{d}r \\
&= \frac{\mathrm{d}}{\mathrm{d}z}\left(\int_0^{R(z)} g\mathrm{d}r\right) - g(z,R(z),t)\frac{\mathrm{d}R(z)}{\mathrm{d}z} + g(z,0,t)\frac{\mathrm{d}0}{\mathrm{d}z} \\
&= \frac{\mathrm{d}}{\mathrm{d}z}\left(\int_S u_z\,\mathrm{d}A\right) - 2\pi R \underbrace{u_z(t,R)}_{=0}\frac{\partial R}{\partial z} \\
&= \frac{\partial Q}{\partial z},
\end{aligned} \tag{65}$$

where we used the definition of Q and that the axial velocity is zero on the vessel wall (no-slip boundary condition).

In summary, with Eqs. (62) and (65), we obtain a one-dimensional mass balance equation in terms of the cross-sectional area $A(z,t)$ and the flow rate $Q(z,t)$ as

$$\frac{\partial A}{\partial t} + \frac{\partial Q}{\partial z} = 0. \tag{66}$$

4.5.3 Momentum balance equations

A detailed derivation might be added here at some point. For the mean time, we refer to the mentioned reference [16, ch.6] and state here only the result, that is the momentum balance equation

$$\frac{\partial Q}{\partial t} + \frac{\partial}{\partial z}\left(\alpha\frac{Q^2}{A}\right) + \frac{A}{\rho}\frac{\partial p}{\partial z} + K_R\frac{Q}{A} = 0, \tag{67}$$

where the dimensionless momentum correction coefficient α encodes the effect of the velocity profile on the nonlinear term and is defined by

$$\alpha := \frac{\int_S v_z^2 \mathrm{d}A}{A\bar{v}^2} = \frac{1}{A}\int_S s^2 \mathrm{d}A, \tag{68}$$

and K_R is the friction function. When assuming a power-law-type velocity profile,

$$v_z(r,z,t) = \bar{v}(z,t)s(r^*) = \bar{v}(z,t)\frac{\gamma+2}{\gamma}\left[1-(r^*)^\gamma\right] = \bar{v}(z,t)\frac{\gamma+2}{\gamma}\left[1-\left(\frac{r}{R}\right)^\gamma\right], \tag{69}$$

K_R and α are given by

$$K_R = -2\pi\frac{\mu}{\rho}s'(1) = 2\pi\frac{\mu}{\rho}(\gamma+2), \quad \gamma = \frac{2-\alpha}{\alpha-1} \tag{70}$$

where $\gamma = 2$ corresponds to a parabolic profile (Poiseuille flow). For the parabolic profile, $\alpha = 4/3$, while for a more flat power-law type profile that is closer to blood flow profiles observed in-vivo, e.g. $\gamma = 9 \Rightarrow \alpha = 1.1$. To simplify the model analysis, it is often assumed that $\alpha = 1$ although this corresponds to a completely flat velocity profile ($\gamma \to \infty$).

4.5.4 Closure model

Summarizing the above derivation, flow in elastic tubes may be derived by the following reduced 1D model

$$\frac{\partial A}{\partial t} + \frac{\partial Q}{\partial z} = 0, \tag{71a}$$

$$\frac{\partial Q}{\partial t} + \frac{\partial}{\partial z}\left(\alpha \frac{Q^2}{A}\right) + \frac{A}{\rho}\frac{\partial p}{\partial z} + K_R \frac{Q}{A} = 0. \tag{71b}$$

On close observation, we see that we have three variables, (Q, A, p), but only two equations. To close the system, that is make the system uniquely solvable, we provide a relation between A and p that essentially models the fluid-structure interaction at the vessel wall. Here, we suggest a simple algebraic relationship, see e.g. [3],

$$p(z,t) = P_{\text{ext}} + \psi(A, A_0, G_0) = P_{\text{ext}} + G_0\left(\sqrt{\frac{A}{A_0}} - 1\right) = P_{\text{ext}} + \frac{\sqrt{\pi} h_0 E}{(1-\nu^2)\sqrt{A_0}}\left(\sqrt{\frac{A}{A_0}} - 1\right), \tag{72}$$

where $E(z)$ denotes Young's modulus (in Pa), ν is the Poisson ratio ($\nu = 0.5$ assuming an incompressible material), $A_0(z)$ is the initial cross-sectional area (for $p = 0$), and $h_0(z)$ is thickness of the vessel wall. The external pressure P_{ext} is the pressure of the extra-vascular tissue. The constant

$$G_0 := \frac{\sqrt{\pi} h_0 E}{(1-\nu^2)\sqrt{A_0}} \tag{73}$$

describes the effective material behavior.

4.5.5 Derivation of the closure model

We can derive the simple algebraic relationship in Eq. (72) from linear elasticity theory (small deformations). This means that we model the arterial wall using the constitutive equations for a (generalized) Hookean material (isotropic, linear-elastic) to relate stresses $\boldsymbol{\sigma}$ and (infinitesimal) strains $\boldsymbol{\epsilon} = \frac{1}{2}\left(\nabla \boldsymbol{u} + \nabla^T \boldsymbol{u}\right)$, denoting with $\boldsymbol{u}$ the displacement. The momentum equations (also called equations of motion), neglecting external body forces, in cylinder coordinates (r, θ, z) are given by

$$\frac{\partial \sigma_{rr}}{\partial r} + \frac{1}{r}\frac{\partial \sigma_{r\theta}}{\partial \theta} + \frac{\partial \sigma_{rz}}{\partial z} + \frac{1}{r}\left(\sigma_{rr} - \sigma_{\theta\theta}\right) = \rho_s \frac{\partial^2 u_r}{\partial t^2}, \tag{74a}$$

$$\frac{\partial \sigma_{r\theta}}{\partial r} + \frac{1}{r}\frac{\partial \sigma_{\theta\theta}}{\partial \theta} + \frac{\partial \sigma_{\theta z}}{\partial z} + \frac{2}{r}\sigma_{r\theta} = \rho_s \frac{\partial^2 u_\theta}{\partial t^2}, \tag{74b}$$

$$\frac{\partial \sigma_{rz}}{\partial r} + \frac{1}{r}\frac{\partial \sigma_{\theta z}}{\partial \theta} + \frac{\partial \sigma_{zz}}{\partial z} + \frac{1}{r}\sigma_{rz} = \rho_s \frac{\partial^2 u_z}{\partial t^2}, \tag{74c}$$

where ρ_s denotes the density of the vessel wall. Matching the assumptions for the 1D model, we seek a symmetric solution such that $\partial/\partial\theta = 0$. Furthermore, we will assume quasi-static conditions such that $\partial^2 \boldsymbol{u}/\partial t^2 \approx 0$, yielding

$$\frac{\partial \sigma_{rr}}{\partial r} + \frac{\partial \sigma_{rz}}{\partial z} + \frac{1}{r}\left(\sigma_{rr} - \sigma_{\theta\theta}\right) = 0, \tag{75a}$$

$$\frac{\partial \sigma_{r\theta}}{\partial r} + \frac{\partial \sigma_{\theta z}}{\partial z} + \frac{2}{r}\sigma_{r\theta} = 0, \tag{75b}$$

$$\frac{\partial \sigma_{rz}}{\partial r} + \frac{\partial \sigma_{zz}}{\partial z} + \frac{1}{r}\sigma_{rz} = 0. \tag{75c}$$

The strain-displacement relation in cylinder coordinates is given by

$$\boldsymbol{\epsilon} = \frac{1}{2}\left(\nabla \boldsymbol{u} + \nabla^T \boldsymbol{u}\right) = \frac{1}{2}\begin{bmatrix} 2\frac{\partial u_r}{\partial r} & \left(\frac{1}{r}\frac{\partial u_r}{\partial \theta} + \frac{\partial u_\theta}{\partial r} - \frac{u_\theta}{r}\right) & \left(\frac{\partial u_r}{\partial z} + \frac{\partial u_z}{\partial r}\right) \\ \left(\frac{1}{r}\frac{\partial u_r}{\partial \theta} + \frac{\partial u_\theta}{\partial r} - \frac{u_\theta}{r}\right) & \frac{2}{r}\left(\frac{\partial u_\theta}{\partial \theta} + u_r\right) & \left(\frac{\partial u_\theta}{\partial z} + \frac{1}{r}\frac{\partial u_z}{\partial \theta}\right) \\ \left(\frac{\partial u_r}{\partial z} + \frac{\partial u_z}{\partial r}\right) & \left(\frac{\partial u_\theta}{\partial z} + \frac{1}{r}\frac{\partial u_z}{\partial \theta}\right) & 2\frac{\partial u_z}{\partial z} \end{bmatrix} \tag{76}$$

$$= \frac{1}{2}\begin{bmatrix} 2\frac{\partial u_r}{\partial r} & \left(\frac{\partial u_\theta}{\partial r} - \frac{u_\theta}{r}\right) & \left(\frac{\partial u_r}{\partial z} + \frac{\partial u_z}{\partial r}\right) \\ \left(\frac{\partial u_\theta}{\partial r} - \frac{u_\theta}{r}\right) & \frac{2u_r}{r} & \frac{\partial u_\theta}{\partial z} \\ \left(\frac{\partial u_r}{\partial z} + \frac{\partial u_z}{\partial r}\right) & \frac{\partial u_\theta}{\partial z} & 2\frac{\partial u_z}{\partial z} \end{bmatrix} \tag{77}$$

where we used again the assumption of axial symmetry in the second equality. The constitutive relations for a Hookean material relate strain and stress as

$$\epsilon_{ij} = \frac{1}{E}\left[(1+\nu)\sigma_{ij} - \nu\delta_{ij}\sigma_{kk}\right], \tag{78}$$

with Young's modulus E, Poisson ratio ν, and the usual Kronecker symbol δ_{ij} (1 if $i = j$ and 0 otherwise). For $\nu < 0.5$, we can invert the relation, and obtain stresses in terms of strains,

$$\sigma_{ij} = \frac{E}{(1+\nu)}\left[\epsilon_{ij} + \frac{\nu}{(1-2\nu)}\delta_{ij}\epsilon_{kk}\right]. \tag{79}$$

A simple force balance at a vessel cross-section at two virtual cuts (one through an axial symmetry plane and

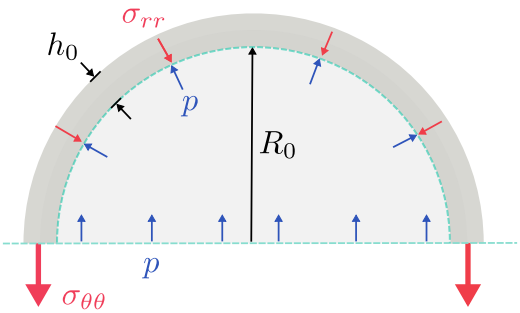

Figure 2: A radial and circumferential cut through a vessel to visualize the forces.

one along the fluid-wall interface, see Fig. 2) shows that

$$F_{p\theta} = 2R_0 p = 2h_0\sigma_{\theta\theta} = F_{\sigma\theta} \qquad \text{and} \qquad F_{pr} = \pi R_0 p = -\pi R_0\sigma_{rr} = F_{\sigma r} \tag{80}$$

$$\Rightarrow \sigma_{\theta\theta} = \frac{pR_0}{h_0} \qquad\qquad \Rightarrow \sigma_{rr} = -p \tag{81}$$

If we assume that $h_0 \ll R_0$, we have that $\sigma_{rr} \ll \sigma_{\theta\theta}$ and on an axial vessel section, we can estimate that $\sigma_{rr} \ll \sigma_{zz}$. We call the situation where the normal stress in one direction is much smaller than in the other direction a plane stress state (here: $\sigma_{rr} \approx 0$). For a resting fluid at pressure p, we can directly compute $\sigma_{zz} = -\frac{pR_0}{2h_0}$ from a force balance. However, when the fluid is moving, it will cause an additional shear force at the fluid-wall interface depending on the velocity profile and fluid material properties. To simplify our model, we will instead make the additional assumption that the vessel is pre-streched in the axial direction and axial displacements are negligibly small and hence $\epsilon_{zz} \approx 0$.

From Eq. (78), we have

$$\epsilon_{\theta\theta} = \frac{1}{E}\left[\sigma_{\theta\theta} - \nu\left(\sigma_{rr} + \sigma_{zz}\right)\right] \approx \frac{1}{E}\left[\sigma_{\theta\theta} - \nu\sigma_{zz}\right], \tag{82}$$

$$\epsilon_{zz} = \frac{1}{E}\left[\sigma_{zz} - \nu\left(\sigma_{\theta\theta} + \sigma_{rr}\right)\right] \approx \frac{1}{E}\left[\sigma_{zz} - \nu\sigma_{\theta\theta}\right] \approx 0. \tag{83}$$

Inserting the second in the first equation eliminates the dependence of $\epsilon_{\theta\theta}$ on $\sigma_z z$ (which is non-zero in this model),

$$\epsilon_{\theta\theta} \approx \frac{1}{E}\left[\sigma_{\theta\theta} - \nu^2\sigma_{\theta\theta}\right] = \frac{(1-\nu^2)}{E}\sigma_{\theta\theta} = \frac{(1-\nu^2)}{E}\frac{pR_0}{h_0}. \tag{84}$$

So far we have assumed that p is the overpressure with respect to some reference pressure outside the vessel. By replacing p with $\Delta p = p - P_{ext}$, we can generalize our considerations for a given non-zero external pressure P_{ext}. Then, solving Eq. (84) for p, we obtain

$$p = P_{ext} + \frac{Eh_0}{(1-\nu^2)R_0}\epsilon_{\theta\theta} = P_{ext} + \frac{Eh_0}{(1-\nu^2)R_0}\frac{R-R_0}{R_0} = P_{ext} + \frac{\sqrt{\pi}Eh_0}{(1-\nu^2)\sqrt{A_0}}\left(\sqrt{\frac{A}{A_0}} - 1\right) \tag{85}$$

where we used Eq. (77) and $A_0 = \pi R_0^2$. □

4.5.6 Conservative form

Theorem 1 (Conservative form)**.** *Equations* (71a)*,* (71b) *and* (72) *can be written in conservation form*

$$\frac{\partial \boldsymbol{U}}{\partial t} + \frac{\partial \boldsymbol{F}(\boldsymbol{U})}{\partial z} + \boldsymbol{S}(\boldsymbol{U}) = 0, \quad \textit{where} \quad \boldsymbol{U} = \begin{bmatrix} A \\ Q \end{bmatrix} \tag{86}$$

are the conserved quantities and the flux and source functions are given by

$$\boldsymbol{F}(\boldsymbol{U}) = \begin{bmatrix} Q \\ \alpha \frac{Q^2}{A} + C_1 \end{bmatrix}, \quad \boldsymbol{S}(\boldsymbol{U}) = \begin{bmatrix} 0 \\ K_R \frac{Q}{A} + \frac{A}{\rho} B_1 - B_2 \end{bmatrix}, \quad C_1 := \int_{A_0}^{A} c_1^2(\tilde{A}) d\tilde{A}, \quad c_1 := \sqrt{\frac{A}{\rho} \frac{\partial \psi}{\partial A}}, \tag{87}$$

$$B_1 := \frac{\partial \psi}{\partial A_0} \frac{\partial A_0}{\partial z} + \frac{\partial \psi}{\partial G_0} \frac{\partial G_0}{\partial z}, \quad B_2 := \frac{\partial C_1}{\partial A_0} \frac{\partial A_0}{\partial z} + \frac{\partial C_1}{\partial G_0} \frac{\partial G_0}{\partial z}. \tag{88}$$

Proof. The mass balance equation Eq. (71a) is already in conservative form and is the first component of the vector-valued representation. Using the definition of the pressure and the functions c_1 and B_1, we have

$$\frac{A}{\rho} \frac{\partial p}{\partial z} = \frac{A}{\rho} \frac{\partial \psi}{\partial z} = \frac{A}{\rho} \left(\frac{\partial \psi}{\partial A} \frac{\partial A}{\partial z} + \frac{\partial \psi}{\partial A_0} \frac{\partial A_0}{\partial z} + \frac{\partial \psi}{\partial G_0} \frac{\partial G_0}{\partial z} \right) \tag{89}$$

$$= c_1^2 \frac{\partial A}{\partial z} + \frac{A}{\rho} \left(\frac{\partial \psi}{\partial A_0} \frac{\partial A_0}{\partial z} + \frac{\partial \psi}{\partial G_0} \frac{\partial G_0}{\partial z} \right) = c_1^2 \frac{\partial A}{\partial z} + \frac{A}{\rho} B_1, \tag{90}$$

by chain rule. Moreover, we have

$$\frac{\partial C_1}{\partial z} = \frac{\partial C_1}{\partial A} \frac{\partial A}{\partial z} + \frac{\partial C_1}{\partial A_0} \frac{\partial A_0}{\partial z} + \frac{\partial C_1}{\partial G_0} \frac{\partial G_0}{\partial z}, \tag{91}$$

and

$$\frac{\partial C_1}{\partial A} = \frac{\partial}{\partial A} \left(\int_{A_0}^{A} c_1^2(\tilde{A}) \mathrm{d}\tilde{A} \right) = \frac{\partial \left(F(A) - F(A_0) \right)}{\partial A} = c_1^2(A), \tag{92}$$

where $F(A)$ denotes the antiderivative of $c_1^2(A)$ for which we know by definition that $\partial F / \partial A = c_1^2$. Inserting Eq. (92) into Eq. (91) yields

$$c_1^2 \frac{\partial A}{\partial z} = \frac{\partial C_1}{\partial z} - \left(\frac{\partial C_1}{\partial A_0} \frac{\partial A_0}{\partial z} + \frac{\partial C_1}{\partial G_0} \frac{\partial G_0}{\partial z} \right) = \frac{\partial C_1}{\partial z} - B_2, \tag{93}$$

and inserting Eq. (93) into Eq. (90) finally yields the expression needed to show the equality proposed in the theorem,

$$\frac{A}{\rho} \frac{\partial p}{\partial z} = \frac{\partial C_1}{\partial z} + \frac{A}{\rho} B_1 - B_2. \tag{94}$$

□

For the area-pressure relationship in Eq. (72), we have

$$c_1 = \sqrt{\sqrt{\frac{A}{A_0} \frac{G_0}{2\rho}}} = \sqrt{\frac{G_0}{2\rho}} \left(\frac{A}{A_0} \right)^{\frac{1}{4}}, \quad C_1 = \int_{A_0}^{A} \frac{G_0}{2\rho} \left(\frac{\tilde{A}}{A_0} \right)^{\frac{1}{2}} \mathrm{d}\tilde{A} = \frac{G_0}{3\rho} A_0 \left(\left(\frac{A}{A_0} \right)^{\frac{3}{2}} - 1 \right). \tag{95}$$

The function c_1 has units of $\mathrm{m\,s^{-1}}$ and has physical significance as a characteristic pressure wave propagation speed of the system.

The equations simplify considerably if A_0 and G_0 can be assumed to be constants (independent of z). Then,

$$\boldsymbol{F}(\boldsymbol{U}) = \begin{bmatrix} Q \\ \alpha \frac{Q^2}{A} + C_1 \end{bmatrix} = \begin{bmatrix} Q \\ \alpha \frac{Q^2}{A} + \frac{G_0}{3\rho} A_0 \left(\frac{A}{A_0} \right)^{\frac{3}{2}} \end{bmatrix}, \quad \boldsymbol{S}(\boldsymbol{U}) = \begin{bmatrix} 0 \\ K_R \frac{Q}{A} \end{bmatrix}. \tag{96}$$

Note that in the second equality, when inserting the expression for C_1, we dropped the constant bit which has a zero derivative with respect to z.

4.6 Linearized 1D model

Equations (71a), (71b) and (72) constitute a nonlinear model in the primary variables A and Q. A simplified model can be obtained in the case of small deformations and flow rates. Such a model is interesting for modelling flow in smaller vessels. Any nonlinear function can be approximated locally around a given point by a linear function (taking the first two terms of the Taylor series developed at that point). In the following, we linearize the functions $\boldsymbol{F}(\boldsymbol{U})$ and $\boldsymbol{S}(\boldsymbol{U})$ around $\boldsymbol{U}_0 = [A_0, 0]^T$ (cf. [11]). To this end, we introduce new state variables a and q as perturbations from the base state $\boldsymbol{U}_0$ such that

$$\boldsymbol{U} = \begin{bmatrix} A \\ Q \end{bmatrix} = \begin{bmatrix} A_0 \\ 0 \end{bmatrix} + \begin{bmatrix} a \\ q \end{bmatrix} = \boldsymbol{U}_0 + \boldsymbol{U}_1 \tag{97}$$

We start with the Taylor series expansion of $\boldsymbol{F}(\boldsymbol{U})$ around $\boldsymbol{U}_0$, given by

$$\boldsymbol{F}(\boldsymbol{U}) = \boldsymbol{F}(\boldsymbol{U}_0) + \boldsymbol{J}_F(\boldsymbol{U}_0)(\boldsymbol{U} - \boldsymbol{U}_0) + O(\boldsymbol{U}^2) = \boldsymbol{F}(\boldsymbol{U})(\boldsymbol{U}_0) + \boldsymbol{J}_F(\boldsymbol{U}_0)\boldsymbol{U}_1 + O(\boldsymbol{U}^2) \tag{98}$$

where $\boldsymbol{J}_F = \partial F_i / \partial U_j$ denotes the Jacobian matrix. We neglect all quadratic and higher order terms.

$$\boldsymbol{F}(\boldsymbol{U}) \approx \boldsymbol{F}(\boldsymbol{U}_0) + \boldsymbol{J}_F(\boldsymbol{U}_0)\boldsymbol{U}_1 = \boldsymbol{0} + \begin{bmatrix} 0 & 1 \\ \frac{G_0}{2\rho} & 0 \end{bmatrix} \begin{bmatrix} a \\ q \end{bmatrix} \tag{99}$$

We do the same for the source term, arriving at

$$\boldsymbol{S}(\boldsymbol{U}) \approx \boldsymbol{S}(\boldsymbol{U}_0) + \boldsymbol{J}_S(\boldsymbol{U}_0)\boldsymbol{U}_1 = \boldsymbol{0} + \begin{bmatrix} 0 & 0 \\ 0 & \frac{K_R}{A_0} \end{bmatrix} \begin{bmatrix} a \\ q \end{bmatrix}. \tag{100}$$

Replacing the nonlinear flux and source term by their linear approximations, we obtain the linear equation system

$$\frac{\partial a}{\partial t} + \frac{\partial q}{\partial z} = 0, \tag{101a}$$

$$\frac{\partial q}{\partial t} + \frac{\partial}{\partial z}\left(\frac{G_0}{2\rho} a\right) + K_R \frac{q}{A_0} = 0, \tag{101b}$$

in terms of the variables a and q. The linearized area-pressure relationship

$$p(A) \approx p(A_0) + \frac{\partial p}{\partial A} a = P_{\text{ext}} + \frac{G_0}{2A_0} a, \tag{102}$$

gives us a way to reformulate the equation system in terms of p and q

$$\frac{2A_0}{G_0} \frac{\partial p}{\partial t} + \frac{\partial q}{\partial z} = 0, \tag{103a}$$

$$\frac{\partial q}{\partial t} + \frac{\partial}{\partial z}\left(\frac{A_0}{\rho} p\right) + K_R \frac{q}{A_0} = 0. \tag{103b}$$

An often made analogy is between flow in vascular networks and electrical circuits. In this analogy, pressure (p) corresponds to voltage, flow rate (q) to current, compliance ($C_{1\text{D}}$) to capacitance, inertance ($L_{1\text{D}}$) to inductance, and viscous friction ($R_{1\text{D}}$) to electrical resistance. For the following, we will assume that A_0 is constant along a given vessel segment (independent of z). Defining the quantities

$$C_{1\text{D}} := \frac{2A_0}{G_0} = \frac{A_0}{\rho c_1^2(A_0)}, \quad L_{1\text{D}} := \frac{\rho}{A_0}, \quad R_{1\text{D}} := \frac{\rho K_R}{A_0^2}, \tag{104}$$

we can rewrite the linearized 1D model once more, yielding (cf. [11])

$$C_{1\text{D}} \frac{\partial p}{\partial t} + \frac{\partial q}{\partial z} = 0, \tag{105a}$$

$$L_{1\text{D}} \frac{\partial q}{\partial t} + \frac{\partial p}{\partial z} + R_{1\text{D}} q = 0. \tag{105b}$$

It can be seen from the equations and where the defined parameters appear that $C_{1\text{D}}$ (compliance) scales how much blood volume can be stored by pressure-driven elastic deformation, $L_{1\text{D}}$ (inertance) scales how fast the system allows changes in the flow rate, and $R_{1\text{D}}$ (resistance) determines the influence of viscous friction. All quantities appear in a length-specific unit (i.e. per meter vessel length).

4.7 0D lumped-parameter model

We can derive an even simpler model, if changes along the axial direction are considered to propagate fast. In following, we first imagine a single vessel of constant length L modeled by the 1D model of the previous section with parameters $C_{1\mathrm{D}}$, $L_{1\mathrm{D}}$, $R_{1\mathrm{D}}$, A_0, G_0 that are constant along the vessel. We integrate Eq. (105) along the vessel, yielding

$$C_{0\mathrm{D}}\frac{\partial \hat{p}}{\partial t} + q_o - q_i = 0, \tag{106a}$$

$$L_{0\mathrm{D}}\frac{\partial \hat{q}}{\partial t} + p_o - p_i + R_{0\mathrm{D}}\hat{q} = 0. \tag{106b}$$

where we defined

$$\hat{p}(t) := \frac{1}{L}\int_0^L p(z,t)\mathrm{d}z, \quad \hat{q}(t) := \frac{1}{L}\int_0^L q(z,t)\mathrm{d}z, \quad C_{0\mathrm{D}} := C_{1\mathrm{D}}L, \quad L_{0\mathrm{D}} := L_{1\mathrm{D}}L, \quad R_{0\mathrm{D}} := R_{1\mathrm{D}}L, \tag{107}$$

and q_i, p_i denote flow rate and pressure at the inlet ($z = 0$) and q_o, p_o denote flow rate and pressure at the outlet ($z = L$) of the vessel.

Let us now assume that we know some given boundary conditions, for example for p_i (pressure at inlet) and q_o (flow rate at outlet). Then, Eq. (106) is a system of two equations and four unknowns $(p_o, q_i, \hat{p}, \hat{q})$. That means, to solve our system we need two closure relation. We follow Milišić and Quarteroni [11] and make the major assumption that $\hat{p} = p_o$ and $\hat{q} = q_i$. This is justified by the observation that since pressure and flow rate do not change much along the vessel (this was already assumed to derive the 1D model), the vessel averages $\hat{p}$ and $\hat{q}$ will be very close to the end point values. Inserting the closure conditions, yields with

$$C_{0\mathrm{D}}\frac{\partial p_o}{\partial t} - q_i = -q_0, \tag{108a}$$

$$L_{0\mathrm{D}}\frac{\partial q_i}{\partial t} + p_o + R_{0\mathrm{D}}q_i = p_i, \tag{108b}$$

a solvable equation system in terms of the unknowns (p_o, q_i).

Note that for other boundary conditions, e.g. given p_o and q_i, we might have chosen the other end points to approximate the averages. This yields a similar but slightly different 0D model.

We can imagine a vessel modeled this way in terms of the following electrical circuit diagram. The position

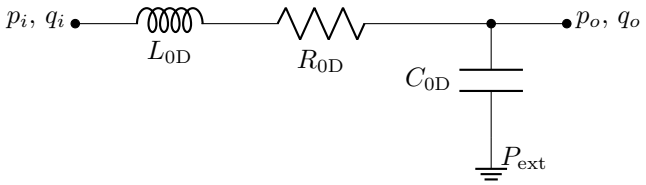

of the capacitor depends on whether the closure relation assumes $\hat{p}$ to be equal to the inlet or the outlet pressure, and we show here the case $\hat{p} \approx p_o$. More details can be found, for example, in [11].

0D model as boundary condition for 1D models. We may also interpret the model given by Eq. (106) more loosely as applying the an entire section of the vascular network. In this interpretation, the coefficients $C_{0\mathrm{D}}$, $L_{0\mathrm{D}}$, $R_{0\mathrm{D}}$ loose their direct compatibility with the coefficients for a single vessel segment but are to be understood in the same physical meaning representing compliance, inertance, and friction of the represented part of the vascular network. We call this approach lumped parameter approach, since the coefficients of an entire group of vessels is lumped into a single coefficient. Interpreted in this way, the 0D model is useful to define meaningful boundary conditions for 1D models, so that we do not have to explicitly represent the entire vascular network tree.

4.8 1D and 0D models for non-pulsatile flow in small vessels

In smaller vessel, it can be a good assumption that possible pressure changes only occur over long time scales much larger than the fluctuations of the heart beat. Due to the compliance of the upstream vessels (Windkessel

effect), fluctuations in the flow rate are small and we have quasi-steady-state conditions, i.e. $\partial q/\partial t = 0$. Flow is described well by the Stokes equations. We may therefore use the following simplified 1D model:

$$C_{1\mathrm{D}}\frac{\partial p}{\partial t} + \frac{\partial q}{\partial z} = 0, \tag{109a}$$

$$\frac{\partial p}{\partial z} + R_{1\mathrm{D}} q = 0. \tag{109b}$$

The equations may be combined into a single equation

$$C_{1\mathrm{D}}\frac{\partial p}{\partial t} - \frac{1}{R_{1\mathrm{D}}}\frac{\partial p^2}{\partial z^2} = 0. \tag{110a}$$

Again, we can also derive a 0D model by integration over the axial direction and obtain

$$C_{0\mathrm{D}}\frac{\partial \hat{p}}{\partial t} + q_o - q_i = 0, \tag{111a}$$

$$p_o - p_i + R_{0\mathrm{D}}\hat{q} = 0, \tag{111b}$$

which corresponds to a simplified electrical circuit. The position of the capacitor depends on whether the closure

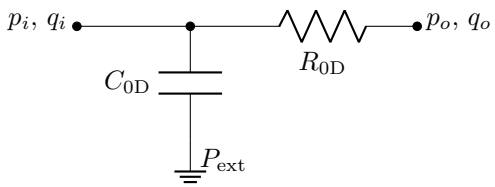

relation assumes $\hat{p}$ to be equal to the inlet or the outlet pressure, and we show here the case $\hat{p} \approx p_i$. More details can be found, for example, in [11].

4.9 Tube flow in (leaky) capillary vessels

In the capillaries, there are several particularities to consider. First, as the red blood cell diameter approaches the vessel diameter, two-phase effects need to be considered. To this end, we may use a model for the apparent viscosity accounting for the strongly non-Newtonian behaviour of blood at this scale. Moreover, we can model additional phase separation effects (Fåhræus effect, Zweifach-Fung bifurcation rule) by accounting for variable hematocrit, or by modeling the two phases separately. The two-phase model with explicit red blood cell tracking and variable hematocrit will not be discussed here. Secondly, capillaries exchange fluids, solvents and particles with the surrounding extra-vascular space over the vessel wall.

We start the derivation with Eqs. (19) to (21), that is the incompressible Navier-Stokes equations in cylinder coordinates, neglecting the circumferential velocity components and gradients. Because we have assume small Reynolds numbers ($\mathrm{Re} \ll 1$), we can neglect the nonlinear terms and inertial terms, arriving at the following form of the Stokes equations

$$\frac{1}{\rho}\frac{\partial p}{\partial r} - \frac{\hat{\mu}_B}{\rho}\left(\frac{1}{r}\frac{\partial}{\partial r}\left(r\frac{\partial v_r}{\partial r}\right) + \frac{\partial^2 v_r}{\partial z^2}\right) = 0, \tag{112}$$

$$\frac{1}{\rho}\frac{\partial p}{\partial z} - \frac{\hat{\mu}_B}{\rho}\left(\frac{1}{r}\frac{\partial}{\partial r}\left(r\frac{\partial v_z}{\partial r}\right) + \frac{\partial^2 v_z}{\partial z^2}\right) = 0, \tag{113}$$

$$\frac{1}{r}\frac{\partial (r v_r)}{\partial r} + \frac{\partial v_z}{\partial z} = 0, \tag{114}$$

where $\hat{mu}_B$ is the apparent dynamic viscosity (in Pa s) and accounts for non-Newtonian effects. For the mass balance Eq. (114), we start as in Section 4.5.3 by integration over the cross-section $S(z,t)$,

$$\int_S \frac{1}{r}\frac{\partial (r v_r)}{\partial r}\,\mathrm{d}A + \int_S \frac{\partial v_z}{\partial z}\,\mathrm{d}A = 0. \tag{115}$$

Then, for the first integral we find that

$$\int_S \frac{1}{r}\frac{\partial(rv_r)}{\partial r}\,\mathrm{d}A = \int_0^{2\pi}\int_0^R \frac{\partial(rv_r)}{\partial r}\mathrm{d}r\mathrm{d}\theta = 2\pi R v_r(z,R), \tag{116}$$

where we used integration by parts. Different from the large vessel, we now make the assumption that the area A is constant in time, i.e. $A = A_0$. However, the vessel wall is assumed to be leaky, that is fluid can cross the vessel wall with the velocity $v_r(z,R) := v_R(z)$. The second term is treated the same way as in Section 4.5.3 and we arrive at

$$\frac{\partial Q(z)}{\partial z} = -2\pi R v_R(z). \tag{117}$$

We note that the mass balance my be derived under less restrictive assumption, that is without assuming radially symmetry velocity profiles. Then, v_R corresponds to the average radial velocity on the cross-section perimeter. The terms in the momentum balance equations are treated the same way as for the 1D model for pulsatile flow, arriving at a similar model,

$$\frac{A_0}{\rho}\frac{\partial p}{\partial z} + K_R\frac{Q}{A_0} = 0 \quad \Rightarrow\ Q = -\frac{A_0^2}{\rho K_R}\frac{\partial p}{\partial z}, \tag{118}$$

which can be solved for Q and inserted into Eq. (117),

$$-\frac{\partial}{\partial z}\left(\frac{A_0^2}{\rho K_R}\frac{\partial p}{\partial z}\right) = -2\pi R v_R(z), \tag{119}$$

obtaining a stationary single equation model in terms of the fluid pressure $p(z)$. Assuming a power-law type velocity profile, we have

$$-\frac{\partial}{\partial z}\left(\frac{\rho}{\mu_B}\frac{\pi R^4}{2(\gamma+2)}\frac{\partial p}{\partial z}\right) = -\rho 2\pi R v_R(z), \tag{120}$$

where μ_B is the mean apparent dynamic viscosity. To solve Eq. (120) in terms of $p(z)$, we need to find closure relations defining μ_B and $v_R(z)$.

4.9.1 Apparent viscosity in small vessels

An empirical model for the apparent viscosity in small vessels based on in-vitro experimental data (in glass tubes) from several studies has been proposed by Pries et al. [13]. It provides a relationship for the apparent viscosity depending on the vessel diameter and the tube hematocrit, H_T. Due to the Fåhræus effect, the tube hematocrit H_T differs from the discharge hemtocrit H_D (bulk blood hematocrit in a reservoir), and the relationship proposed by [12] is

$$\frac{H_T}{H_D} = H_D + (1-H_D)\left(1 + 1.7e^{-0.415D} - 0.6e^{-0.011D}\right), \tag{121}$$

where $D = 2R$ is the vessel diameter. This was obtained for human blood samples where the mean red blood cell volume is $V_{\mathrm{RBC}}^{\mathrm{hum}} = 92\times10^{-18}\,\mathrm{m}^3 = 92\,\mathrm{fL}$. According to Pries and Secomb [15], a relation for other species with different red blood cell volume may be obtained by multiplying the vessel diameters in the equation by a factor $(V_{\mathrm{RBC}}^{\mathrm{hum}}/V_{\mathrm{RBC}}^{\mathrm{s}})^{1/3}$. For rat blood with $V_{\mathrm{RBC}}^{\mathrm{rat}} = 55\,\mathrm{fL}$, this gives a factor of 1.187 [12].

The apparent dynamic viscosity μ_B is given by

$$\eta^{\mathrm{vitro}} := \frac{\mu_B^{\mathrm{vitro}}}{\mu_P} = 1 + (\eta_{0.45}^{\mathrm{vitro}} - 1)\frac{(1-H_D)^C - 1}{(1-0.45)^C - 1}, \tag{122}$$

$$\eta_{0.45}^{\mathrm{vitro}}(D) = 220e^{-1.3D} - 2.44e^{-0.06D^{0.645}} + 3.2, \tag{123}$$

$$C(D) = (0.8 + e^{-0.075D})\left(\frac{1}{1+10^{-11}D^{12}} - 1\right) + \frac{1}{1+10^{-11}D^{12}}, \tag{124}$$

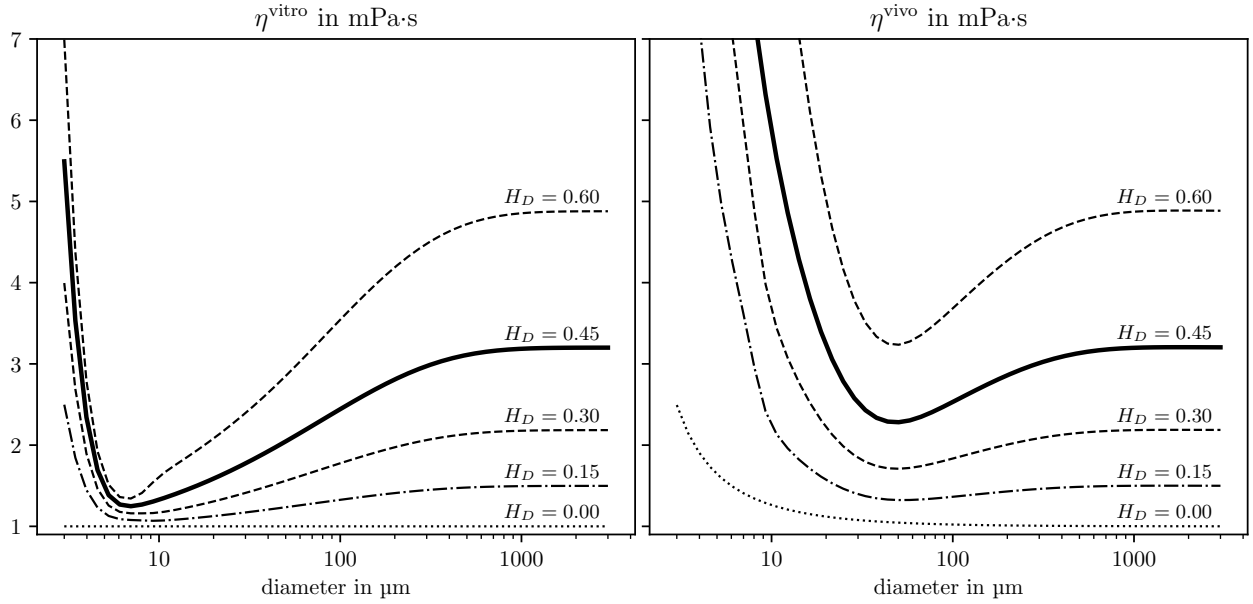

Figure 3: Relative apparent dynamic viscosity in the microvasculature depending on vessel diameter and discharge hematocrit according to the empirical in-vitro model found by Pries et al. [12] (left) and the empirical in-vivo model proposed by Pries et al. [14] scaled for human blood with mean red blood cell volume $V_{\text{RBC}}^{\text{hum}} = 92\,\text{fL}$. The figure can be reproduced with the Python script `plot_viscosity.py`.

where $\eta_{0.45}$ is the relative apparent viscosity at a discharge hematocrit of $H_D = 0.45$, C is a scaling function, and μ_P is the dynamic viscosity of blood plasma ($\mu_P \approx 1.1\,\text{mPa s}$) which is modeled as a Newtonian fluid.

Due to the anatomical complexity of vessels in-vivo, in particular the existence of the so-called endothelial surface layer that results in a apparent cell-free layer of about 0.1 µm to 2 µm, the apparent viscosity has been found to deviate from the law proposed for glass tubes when investigated in-vivo (in living rats) [14]. Pries et al. [14] therefore propose a scaled in-vivo viscosity law given by

$$\eta^{\text{vivo}} := \frac{\mu_B^{\text{vivo}}}{\mu_P} = \left[1 + (\eta_{0.45}^{\text{vivo}} - 1)\frac{(1-H_D)^C - 1}{(1-0.45)^C - 1}\left(\frac{D}{D-1.1}\right)^2\right]\left(\frac{D}{D-1.1}\right)^2, \tag{125}$$

$$\eta_{0.45}^{\text{vivo}}(D) = 6e^{-0.085D} - 2.44e^{-0.06D^{0.645}} + 3.2, \tag{126}$$

and C is the same as for the in-vitro law above, i.e. Eq. (124).

The apparent viscosity relationship are shown in Fig. 3. For more information on the derivation, historical context and flow in microvascular networks in general, we refer to the review article by Pries and Secomb [15].

4.9.2 Flow across the vascular wall

The capillary wall consists mostly of the endothelial cell layer (see Fig. 4) that has various gaps and pores depending on the type of capillary. The most common model used for fluid flow across the capillary vessel wall is Starling's law due to Starling [17]. It proposes that the filtration velocity v_R (in m s^{-1}) is proportional to the hydrostatic pressure difference and the so-called oncotic pressure (an osmotic pressure exerted by large proteins present in the blood stream such as albumin) across the vessel wall,

$$v_R(z) = L_p(p - P_{\text{ext}} - \sigma_w \Delta\Pi), \tag{127}$$

where p denotes the fluid pressure inside the capillary, P_{ext} is the mean fluid pressure right outside the capillary (on the green surface in Fig. 4), L_p is the filtration coefficient (in $\text{m Pa}^{-1}\,\text{s}^{-1}$), $\Delta\Pi$ is the oncotic pressure difference across the vessel wall, and σ_w is the osmotic reflection coefficient that is close to 1 for large molecules that occur in relatively high concentrations in the blood stream such as albumin and close to 0.1 for small molecules present in low concentration, with the notable exception of the brain where it can be mostly assumed

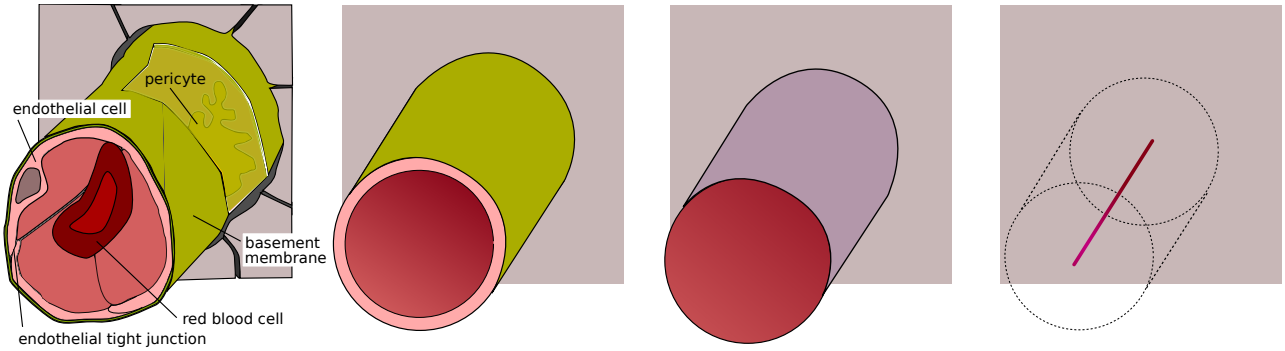

Figure 4: Step-wise model reduction shown for a continuous capillary. After idealizing the geometry, the vessel wall is reduced to a sharp interface. Integration over cross-sections yields a 1D model of blood flow. Figure reproduced from [9].

to be close to 1 [7]. Baxter and Jain [2], Jain et al. [8] estimate L_p to be between $2.4 \times 10^{-12}\,\mathrm{m\,Pa^{-1}\,s^{-1}}$ (in normal rat skeletal muscle capillaries) and $1.4 \times 10^{-10}\,\mathrm{m\,Pa^{-1}\,s^{-1}}$ (in tumors). Measurements for the other quantities in different species are, for example, summarized by Levick [10]. We can use Eq. (127) to replace v_R in the right-hand-side of Eq. (120).

5 Numerical methods

This is a brief introduction to Finite Volume Methods with the goal of showing how to discretize and solve some of the blood flow models derived in the previous sections along vessel segments.

5.1 The Finite Volume Method

We start by looking at a simple linear scalar conservation equation,

$$\frac{\partial c}{\partial t} + \operatorname{div}(\boldsymbol{v}c) = 0, \tag{128}$$

in a bounded spatial domain $\Omega \subset \mathbb{R}^d$ and a time interval $[0, t_{\mathrm{End}}]$, where $c : \Omega \times [0, t_{\mathrm{End}}] \to \mathbb{R}$ denotes a scalar concentration field that evolves over time. The concentration field is transported by advection in a bulk fluid moving at steady velocity field $\boldsymbol{v} : \Omega \to \mathbb{R}^d$ (for example, the blood flow velocity). The concentration field is fully described by Eq. (128) together with an initial state $c(\boldsymbol{x}, 0) = c_0(\boldsymbol{x})$, and boundary conditions on the inflow boundary. We call the inflow boundary, all parts of $\partial\Omega$ (the boundary of Ω), where $\boldsymbol{v} \cdot \boldsymbol{n}_\Omega < 0$ holds. The vector $\boldsymbol{n}_\Omega$ denotes the unit outward-pointing normal vector on $\partial\Omega$. Because in the type of transport described by Eq. (128) information only flows in one direction (the direction of the velocity field), we do not have to prescribe any boundary conditions on the outflow boundary ($\boldsymbol{v} \cdot \boldsymbol{n}_\Omega \geq 0$). (And we cannot prescribe them since the differential equation together with the inflow boundary conditions and initial conditions already fully determines the solution.)

If we integrate Eq. (128) over some arbitrary control volume region $K \subseteq \Omega$ and apply the divergence theorem,

$$\int_n \frac{\partial c}{\partial t}\mathrm{d}V + \int_n \operatorname{div}(\boldsymbol{v}c)\mathrm{d}V = \int_n \frac{\partial c}{\partial t}\mathrm{d}V + \int_{\partial K} c\boldsymbol{v} \cdot \boldsymbol{n}_K \mathrm{d}A = \frac{\mathrm{d}}{\mathrm{d}t}\int_n c\,\mathrm{d}V + \int_{\partial K} c\boldsymbol{v} \cdot \boldsymbol{n}_K\,\mathrm{d}A = 0, \tag{129}$$

we can conclude that the total amount of the substance in control volume K only changes by the net flux over the boundary ∂K, and therefore, it must be conserved within K. This explains the name *conservation equation* or *conservation law*. The concentration c is the density of the conserved quantity (amount of substance).

For the Finite Volume Method (FVM), we partition the domain into a set $\mathcal{T}$ of (finite polytope) control volumes K ($\mathcal{T}$ is often called a mesh) such that the domain

$$\Omega = \bigcup_{K \in \mathcal{T}} K, \tag{130}$$

is given by the union of all control volumes K in $\mathcal{T}$. This process is called spatial discretization. An example

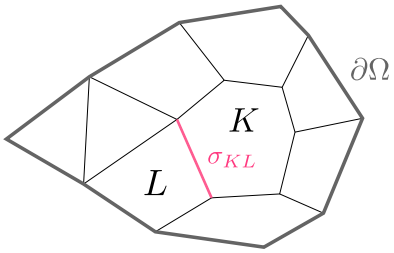

Figure 5: A two-dimensional mesh $\mathcal{T}$ of polygonal control volumes K.

domain is shown in Fig. 5. Each polytope control volume K has a set Σ of facets σ (which have dimension $d-1$) that it shares either with another control volume (inner facets) or with the domain boundary (boundary facets). For example, for one-dimensional domains ($d = 1$) the facets are simply the vertices of a line segment. We also discretize the time domain by splitting the interval into a number of discrete steps starting at $T_0 = [t_0, t_1]$ and denote with $\Delta t_n = t_{n+1} - t_n$, the n-th time step size (a measure of the n-th subinterval). Moreover, we introduce the cell averages

$$c_K = \frac{1}{|K|} \int_K c(\boldsymbol{x}, t) \mathrm{d}V, \tag{131}$$

which will be our discrete unknowns. Note that we have one unknown c_K per control volume K. Integrating Eq. (128) in time and space over control volumes K, yields as many equations as unknowns,

$$\int_{t_n}^{t_{n+1}} \int_K \frac{\partial c}{\partial t} \mathrm{d}V \mathrm{d}t + \int_{t_n}^{t_{n+1}} \int_{\partial K} c\boldsymbol{v} \cdot \boldsymbol{n}_K \, \mathrm{d}A \, \mathrm{d}t = 0. \tag{132}$$

Exchanging the order of integration and using the definition of the cell averages yields

$$|K| c_K^{n+1} - |K| c_K^n + \int_{t_n}^{t_{n+1}} \int_{\partial K} c\boldsymbol{v} \cdot \boldsymbol{n}_K \, \mathrm{d}A \, \mathrm{d}t = 0. \tag{133}$$

Applying an explicit Euler scheme in time, the flux term is approximated by

$$|K| c_K^{n+1} - |K| c_K^n + \Delta t_n \left[\int_{\partial K} c\boldsymbol{v} \cdot \boldsymbol{n}_K \, \mathrm{d}A \right]^n = 0, \tag{134}$$

where $(\cdot)^k$ here means that the expression is evaluated at time t_n. Finally, the continuous flux integral is approximated by numerical fluxes F at each facet σ,

$$|K| c_K^{n+1} - |K| c_K^n + \Delta t_n \sum_{\sigma \in \Sigma} F_{K,\sigma}^n = 0, \tag{135}$$

and we arrive at the fully discretized equations. Due to the explicit Euler discretization, we can formulate a direct update rule

$$c_K^{n+1} = c_K^n - \frac{\Delta t_n}{|K|} \sum_{\sigma \in \Sigma} F_{K,\sigma}^k \tag{136}$$

for each cell unknown, where the right-hand side terms only depend on known quantities at time t_n. Therefore each cell unknown can be updated independently. (In a code implementation, this makes it particularly easy to update cell values in parallel for efficiency.)

5.1.1 Choosing the numerical flux (hyperbolic problems)

The careful construction of the numerical fluxes F is crucial to arrive at a useful numerical solution method. To maintain the conservation property of the continuous equations, we want that for two neighboring control

volumes K and L that share a facet σ_{KL} that $F_{K,\sigma_{KL}} + F_{L,\sigma_{LK}} = 0$. That means that whatever leaves control volume K over facet σ_{KL} will end up in control volume L and vice versa. The scheme is then said to be (locally) *conservative*.

Although this constrains the number of choices, there is still freedom in choosing particular numerical flux formulations. We discuss some examples below for the case of one-dimensional equations. The case $d = 1$ is simply a particular instance of the problem described in the previous section. In the one-dimensional case, Eq. (128) simplifies to

$$\frac{\partial c}{\partial t} + \frac{\partial (vc)}{\partial z} = 0, \tag{137}$$

where c, for example, now describes the cross-section average concentration in a vessel. We can generalize the flux term to some function $f(c)$,

$$\frac{\partial c}{\partial t} + \frac{\partial f(c)}{\partial z} = 0. \tag{138}$$

The one-dimensional mesh is shown in Fig. 6. Integration in space and time, inserting the definition of cell

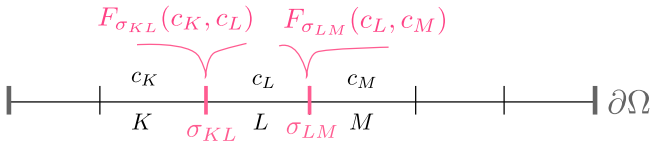

Figure 6: A one-dimensional mesh $\mathcal{T}$ of control intervals K (cells). Unknowns c_i are associated with cells and numerical fluxes are associated with cell facets σ.

averages, and using an explicit Euler scheme in time, yields

$$c_L^{n+1} = c_L^n - \frac{\Delta t_n}{\Delta z_L} \left(F^n_{L,\sigma_{LM}} - F^n_{L,\sigma_{KL}} \right), \tag{139}$$

where $\Delta z_L := |L|$ and the facets are now the two vertices at the end of each control interval K. Here L denotes the element in the middle to be balanced, while K is the element to the left and M is the element to the right.

We define the numerical flux as a function of the left and right state,

$$F^n_{\sigma_{KL}} := F^n_{\sigma_{KL}}(c_K, c_L). \tag{140}$$

The numerical flux is said to be *consistent* if

$$F(a, a) = f(a) \quad \forall a \in \mathbb{R}. \tag{141}$$

We want the scheme to be consistent with the physical behavior of the continuous equation.

A desirable property is that our scheme is *monotone*. A scheme is monotone if it holds that

$$c_K^n \leq u_K^n \quad \forall K \quad \Rightarrow \quad c_K^{n+1} \leq u_K^{n+1} \quad \forall K, \tag{142}$$

for some given discrete solutions c and u. Monotonicity makes sure that the scheme converges to the physical solution (the so-called weak entropy solution). In the physical interpretation, monotonicity makes sure that the entropy of our system cannot increase.

Two slightly weaker definitions are also useful properties. The so-called *total variation* for the discrete equations is defined as

$$TV(c^n) := \sum_{L \in \mathcal{T}} |c_L^n - c_K^n| \tag{143}$$

where the element K is the left neighbor of the element L. The total variation essentially measures oscillations in our solution. (For the left-most element we assume that c_K^n represents some suitable approximation on the inflow boundary.) It is known that physical solutions are *total-variation-diminishing* (TVD). The concept of TVD numerical schemes was introduced by Harten [5]. A numerical scheme is said to be TVD if it holds that

$$TV(c^{n+1}) \leq TV(c^k) \quad \forall t_n. \tag{144}$$

In particular, this also implies that if a solution at time point t_n is monotone, it will remain monotone in all future time steps, that is, TVD schemes are monotonicity-preserving. Consistent TVD schemes are convergent.

All monotone schemes are TVD and therefore monotonicity-preserving. More importantly, it can be shown that consistent and monotone schemes converge against the physical solution (entropy solution).

However, monotone schemes are generally only first-order accurate (consistency error). This is stated by Gudonov's order barrier theorem [4].

Let's look at some examples of numerical fluxes that are consistent:

- $F(a,b) = \frac{f(a)+f(b)}{2}$ (central flux approximation),
- $F(a,b) = \frac{f(a)+f(b)}{2} - \frac{0.5(\Delta z_K + \Delta z_L)}{2\Delta t}$ (Lax-Friedrichs flux approximation),
- $F(a,b) = f(a) \quad \text{for } f' > 0$ (upwind flux approximation / Riemann solver).

The central flux method is second-order accurate but is prone to oscillatory solutions. The second and third schemes are monotone but only first-order accurate. The script `advection.py` compares the different schemes numerically. The result for a test case with $\Delta t = 0.1\Delta z$ and $\Delta z = 1/300$ is shown in Fig. 7. Here we can see that we are faced with a trade-off. Monotone schemes are stable but only first-order accurate. The second-order scheme is more accurate where the solution is smooth but produces unphysical oscillatory solutions with around the shock.

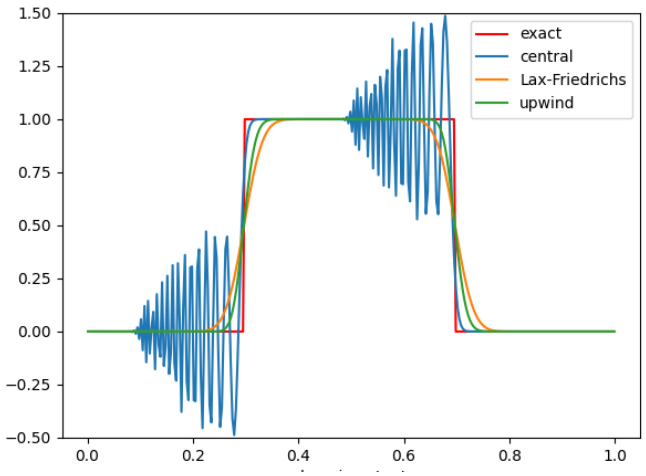

Figure 7: Comparison of the numerical solution obtained with different numerical flux schemes with the exact solution solving the linear advection equation with $v = 1$. Shown is the solution at $t = 0.2$ and the spatial domain is the unit interval. The central flux approximates produces an oscillatory solution. The upwind scheme and the Lax-Friedrichs scheme show a monotone and stable solution and the Lax-Friedrichs scheme shows the largest artificial dissipation.

5.1.2 Flux limiters (shock-capturing methods)

One idea to construct flux limiters is to use the best of two worlds: where the solution is discontinuous, we use a monotone first-order scheme; where the solution is smooth, we use a second-order scheme for increased accuracy. The job of the flux limiters is then to provide a mechanism to automatically detect and switch between these approximations.

Taking a stable first-order numerical flux approximation F_{low} (e.g. the upwind flux approximation) and a higher-order flux numerical approximation F_{high}, a useful family of flux limiters can be written in the form

$$F^n_{\sigma_{LM}} = F^n_{\text{low},\sigma_{LM}} - \zeta(r_L)(F^n_{\text{low},\sigma_{LM}} - F^n_{\text{high},\sigma_{LM}}), \tag{145}$$

where ζ is the flux limiter function and $\zeta(r) \leq 0$, and

$$r_L = \frac{c_L - c_K}{c_L - c_M} \tag{146}$$

is a ratio of gradients of the solution in the mesh. Note that this definition assumes that the transport direction is $K \to L \to M$. This means to approximate the flux at face σ_{LM} we now need, in addition to the neighboring degrees of freedom c_L and c_M the neighbor of the neighboring element in the upstream direction c_K. This means our stencil for computing the flux contributions to element L increases by one (in the upwind direction).

Which flux limiter function should we choose? Many flux limiters are designed to be total-variation-diminishing (TVD). A technique for the construction of second-order TVD schemes is given in [18]. Given that F_{high} is second-order accurate, popular flux limiters (yielding TVD schemes) are given by Eq. (145) and

- $\zeta_{\text{sb}}(r) = \max\{0, \min(2r, 1), \min(r, 2)\}$ ("superbee", $\lim_{r\to\infty} \zeta(r) = 2$),
- $\zeta_{\text{vl}}(r) = (r + |r|)/(1 + |r|)$ ("van Leer", $\lim_{r\to\infty} \zeta(r) = 2$),
- $\zeta_{\text{mm}}(r) = \max\{0, \min(r, 1)\}$ ("minmod", $\lim_{r\to\infty} \zeta(r) = 1$).

The script `advection.py` implements these flux limiters by combining the central and the upwind flux approximation. The improved results over Fig. 7 are shown in Fig. 8. However, note that by introducing flux limiters, we make the flux function nonlinear and increase the stencil size.

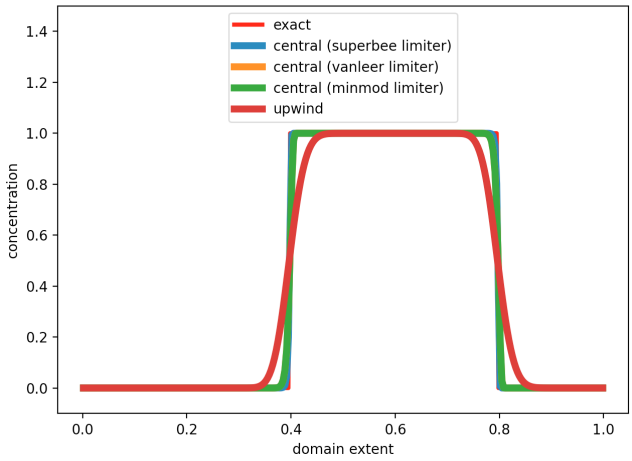

Figure 8: Comparison of the numerical solution obtained with different numerical flux schemes with the exact solution solving the linear advection equation with $v = 1$. Shown is the solution at $t = 0.2$ and the spatial domain is the unit interval. Different flux limiters significantly improve the solution accuracy while capturing the shock.

5.2 Monotone and consistent numerical method for the 1D blood flow model in elastic vessels

We want to solve the equations derived in Section 4.5 for 1D blood flow in elastic vessels in a vessel segment given boundary and initial conditions that will be specified later.

5.2.1 Characteristic variables

For the construction of a Riemann solver it is helpful to make a variable transformation into so-called characteristic variables, which provide information in which direction (sign of eigenvalues) information is transported. To derive these new variables, we first transform Eq. (86) as follows

$$\frac{\partial \boldsymbol{U}}{\partial t} + \frac{\partial \boldsymbol{F}(\boldsymbol{U})}{\partial \boldsymbol{U}} \frac{\partial \boldsymbol{U}}{\partial z} + \boldsymbol{S}(\boldsymbol{U}) = 0, \tag{147}$$

with the Jacobian matrix of the flux function $\boldsymbol{J}(\boldsymbol{U}) := \frac{\partial \boldsymbol{F}(\boldsymbol{U})}{\partial \boldsymbol{U}}$, which is, according to Eq. (96), given as

$$\boldsymbol{J}(\boldsymbol{U}) = \frac{\partial F_i}{\partial U_j} = \begin{pmatrix} 0 & 1 \\ -\bar{v}^2 + c_1^2(A) & 2\bar{v} \end{pmatrix}, \quad \bar{v} := \frac{Q}{A}. \tag{148}$$

The eigenvalues of $\boldsymbol{J}$ can be computed as solutions of the characteristic equation

$$\det\left(\boldsymbol{J}-\lambda\boldsymbol{I}\right)=\lambda^2-2\bar{v}\lambda+\bar{v}^2-c_1^2(A)=(\lambda-\bar{v})^2-c_1^2(A)=(\lambda-\bar{v}+c_1(A))(\lambda-\bar{v}-c_1(A))=0, \tag{149}$$

and are therefore given by

$$\lambda_1=\bar{v}-c_1,\quad \lambda_2=\bar{v}+c_1, \tag{150}$$

and the corresponding left eigenvectors are given by

$$\boldsymbol{l}_1^T\left(\boldsymbol{J}-\lambda_1\boldsymbol{I}\right)=0\;\Rightarrow\;\boldsymbol{l}_1=\frac{1}{A}(\bar{v}+c_1,-1)^T,\quad \boldsymbol{l}_2^T\left(\boldsymbol{J}-\lambda_2\boldsymbol{I}\right)=0\;\Rightarrow\;\boldsymbol{l}_2=\frac{1}{A}(c_1-\bar{v},1)^T. \tag{151}$$

With this eigenbasis the Jacobian matrix can be diagonalized, i.e. $\boldsymbol{J}=\boldsymbol{L}^{-1}\boldsymbol{\Lambda}\boldsymbol{L}$, where the rows of $\boldsymbol{L}$ correspond to the left eigenvectors and $\boldsymbol{\Lambda}:=\mathrm{diag}(\lambda_i)$ is the diagonal matrix of eigenvalues.

Definition 1. *A system of transport equations in the form of Eq.* (147) *is called hyperbolic if the Jacobian matrix of the flux function* $\boldsymbol{J}(\boldsymbol{U}):=\frac{\partial\boldsymbol{F}(\boldsymbol{U})}{\partial\boldsymbol{U}}$ *is diagonalizable and only has real eigenvalues.*

Inserting the eigendecomposition of the Jacobian into Eq. (147) and multiplying with $\boldsymbol{L}$ results in

$$\boldsymbol{L}\frac{\partial\boldsymbol{U}}{\partial t}+\boldsymbol{\Lambda}\boldsymbol{L}\frac{\partial\boldsymbol{U}}{\partial z}+\boldsymbol{L}\boldsymbol{S}(\boldsymbol{U})=0. \tag{152}$$

If we find new variables such that $\frac{\partial W_i}{\partial\boldsymbol{U}}=\boldsymbol{l}_i$ or in vector-notation $\frac{\partial\boldsymbol{W}}{\partial\boldsymbol{U}}=\boldsymbol{L}$, then we deduce a system of coupled scalar transport equations for the characteristic variables:

$$\frac{\partial\boldsymbol{W}}{\partial\boldsymbol{U}}\frac{\partial\boldsymbol{U}}{\partial t}+\boldsymbol{\Lambda}\frac{\partial\boldsymbol{W}}{\partial\boldsymbol{U}}\frac{\partial\boldsymbol{U}}{\partial z}+\boldsymbol{L}\boldsymbol{S}(\boldsymbol{U})=0\;\Leftrightarrow\;\frac{\partial\boldsymbol{W}}{\partial t}+\boldsymbol{\Lambda}\frac{\partial\boldsymbol{W}}{\partial z}+\boldsymbol{L}\boldsymbol{S}(\boldsymbol{U})=0. \tag{153}$$

Thus, calculation of the antiderivatives of $\boldsymbol{l}_1$ and $\boldsymbol{l}_2$ with respect to A and Q gives the new set of variables W_1 and W_2:

$$W_1=-\frac{Q}{A}+4c_1(A),\;W_2=\frac{Q}{A}+4c_1(A). \tag{154}$$

(For this computation, use the definition of $\bar{v}$ and c_1 in terms of Q and A, see Eqs. (95) and (148).) The inverse transformation, i.e. expressing A,Q in terms of W_1,W_2, is given as

$$A(W_1,W_2)=A_0\left(\frac{W_1+W_2}{8c_0}\right)^4,\quad Q(W_1,W_2)=A(W_1,W_2)\left(\frac{W_2-W_1}{2}\right), \tag{155}$$

where $c_0:=c_1(A_0)=\sqrt{G_0/(2\rho)}$. This transformation allows to express $\boldsymbol{L}\boldsymbol{S}(\boldsymbol{U})$ of Eq. (153) in terms of $\boldsymbol{W}=(W_1,W_2)^T$.

5.2.2 Observation

For physiologically sensible conditions, we can make the assumption that $c_1\gg\bar{v}$. This has the physical interpretation that waves (due to fluid-structure interaction) travel faster than the mean blood flow velocity. Consequently, eigenvalue λ_1 is always negative and the eigenvalue λ_2 is always positive. As the eigenvalues λ_1 and λ_2 correspond to the "transport velocities" of the characteristic equations Eq. (153), we can construct a generalized upwind scheme based on this information.

5.2.3 Numerical scheme (Riemann solver)

With the characteristic variables, we have a good understanding of how information is propagated at interfaces (at any given cross-sectional cut). In fact, for physiological blood flow conditions, we know that the characteristic variable W_1 is transported from right to left, while the characteristic variable W_2 is transported from left to right. This information allows us to construct a Riemann solver. A Riemann problem is given at every face σ_{LM} with a left state $\boldsymbol{U}_L$ and a right state $\boldsymbol{U}_M$. The finite volume scheme (omitting the source term for brevity) based on an explicit Euler time discretization results in

$$\boldsymbol{U}_L^{n+1}=\boldsymbol{U}_L^n-\frac{\Delta t_n}{\Delta z_L}\left(F^n_{L,\sigma_{LM}}-F^n_{L,\sigma_{KL}}\right), \tag{156}$$

and therefore our goal is to find a numerical flux $F^n_{L,\sigma_{LM}}$. To this end, we choose

$$F^n_{L,\sigma_{LM}} := F^n_{L,\sigma_{LM}}(\boldsymbol{U}^n_{\sigma_{LM}}(W_1, W_2)). \tag{157}$$

This means we construct a flux based on a consistent approximation $\boldsymbol{U}^n_{\sigma_{LM}}$ on the facet σ_{LM} that we will determine with the characteristic variables. Because of the directionality of the transport using a generalized upwind scheme here means using $W_1 = W^n_{1,M}(\boldsymbol{U}^n_M)$ and $W_2 = W^n_{2,L}(\boldsymbol{U}^n_L)$ to compute $\boldsymbol{U}^n_{\sigma_{LM}}$ by using Eq. (155).

5.2.4 Upwind scheme at bifurcations

We will assume that there is one feeding vessel (I) (where the blood flows towards the bifurcation) that bifurcates (splits in two) into two downstream vessels (II) and (III) in which the blood flows away from the bifurcation, see Fig. 9. For cases where flow directions are different, the following consideration work analogously but signs and directional choices differ. Moreover, we assume that each of the vessels connected to the bifurcation has given parameters A^v_0 and G^v_0, $v \in \{\mathrm{I}, \mathrm{II}, \mathrm{III}\}$. Hence, they may differ (and usually will differ) from vessel to vessel. We assume that the parameter fields are constant per vessel but with a discontinuity across bifurcations.

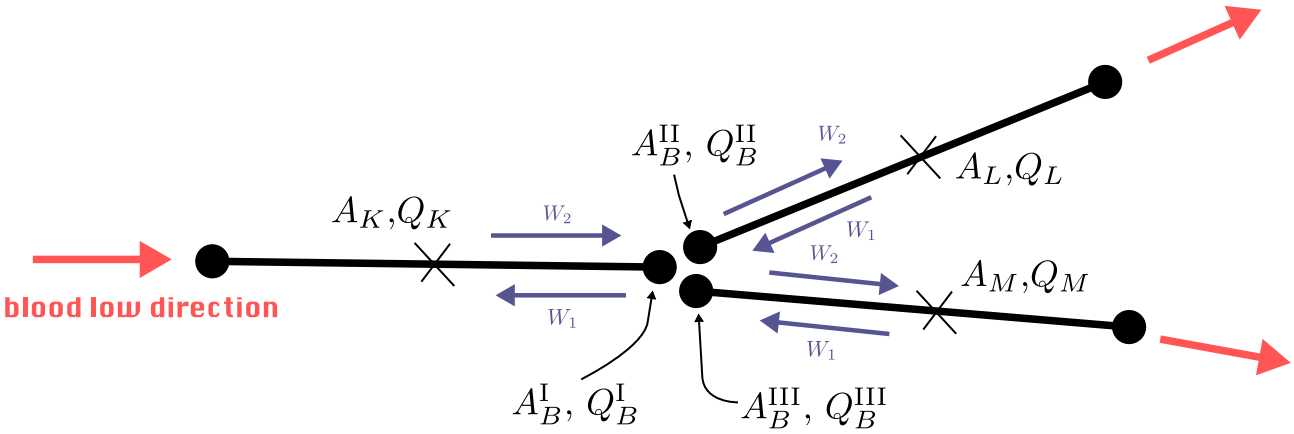

Figure 9: Flow through a bifurcation. Coupling conditions can be derived using a generalized upwind scheme. The bifurcation solver solves for the states at the bifurcation in each vessel, A^{I}_B, A^{II}_B, A^{III}_B, Q^{I}_B, Q^{II}_B, Q^{III}_B.

To evaluate the flux function $\boldsymbol{F}(\boldsymbol{U})$ at the bifurcation in each vessel, we need to approximate $\boldsymbol{U}^v_B$, where $v \in \{\mathrm{I}, \mathrm{II}, \mathrm{III}\}$ and the subscript B stands for "bifurcation" signifying that the element face at which these quantities are approximated is located in the bifurcation.

Recall that $\boldsymbol{U} = (A, Q)^T$ and that we have three vessels at the bifurcation, we conclude that we are looking for six unknowns, A^{I}_B, A^{II}_B, A^{III}_B, Q^{I}_B, Q^{II}_B, Q^{III}_B. You may think of the element faces at the bifurcation to exist three times, once for each vessel, and our goal is to evaluate the fluxes $\boldsymbol{F}^{\mathrm{I}}_B(A^{\mathrm{I}}_B, Q^{\mathrm{I}}_B)$, $\boldsymbol{F}^{\mathrm{II}}_B(A^{\mathrm{II}}_B, Q^{\mathrm{II}}_B)$, $\boldsymbol{F}^{\mathrm{III}}_B(A^{\mathrm{III}}_B, Q^{\mathrm{III}}_B)$ which appear in a finite volume scheme when balancing the elements in the grid adjacent to the bifurcation. We also introduce the element unknowns $\boldsymbol{U}_K$, $\boldsymbol{U}_L$, $\boldsymbol{U}_M$, where K is the element next to the bifurcation in vessel (I), L in vessel (II) and M (III).

As a first condition, we recall that mass is conserved at the bifurcation and therefore

$$Q^{\mathrm{I}}_B = Q^{\mathrm{II}}_B + Q^{\mathrm{III}}_B. \tag{158}$$

Moreover, we know from Bernoulli's principle that a velocity increase of fluid leads simultaneously to a decrease in static pressure or a decrease in the fluid's potential energy. For incompressible fluids (ρ = const.) this principle can be summarized as

$$\frac{1}{2}\rho\bar{v}^2 + \rho g z + p = \text{const.}$$

We recall that we neglected gravitational forces and therefore, here

$$p_t := \frac{1}{2}\rho\bar{v}^2 + p = \text{const.},$$

where p_t is sometimes called total pressure (the sum of the static pressure p and the dynamic pressure $\frac{1}{2}\rho\bar{v}^2$). (We remark that for capillary vessels, where the flow velocities are very small (creeping flow assumption, Re $\ll 1$), the dynamic pressure is usually considered negligible in comparison to the static pressure.) In effect, Bernoulli's principle states that the total pressure is continuous across the bifurcation (even though, for instance, the cross-sectional area is discontinuous). This gives us two more conditions

$$p^{\mathrm{I}}_{t,B} = p^{\mathrm{II}}_{t,B} \quad \Rightarrow \quad \frac{1}{2}\left(\frac{Q^{\mathrm{I}}_B}{A^{\mathrm{I}}_B}\right)^2 + 2(c^{\mathrm{I}}_0)^2\left(\sqrt{\frac{A^{\mathrm{I}}_B}{A^{\mathrm{I}}_0}} - 1\right) = \frac{1}{2}\left(\frac{Q^{\mathrm{II}}_B}{A^{\mathrm{II}}_B}\right)^2 + 2(c^{\mathrm{II}}_0)^2\left(\sqrt{\frac{A^{\mathrm{II}}_B}{A^{\mathrm{II}}_0}} - 1\right), \tag{159}$$

$$p^{\mathrm{I}}_{t,B} = p^{\mathrm{III}}_{t,B} \quad \Rightarrow \quad \frac{1}{2}\left(\frac{Q^{\mathrm{I}}_B}{A^{\mathrm{I}}_B}\right)^2 + 2(c^{\mathrm{I}}_0)^2\left(\sqrt{\frac{A^{\mathrm{I}}_B}{A^{\mathrm{I}}_0}} - 1\right) = \frac{1}{2}\left(\frac{Q^{\mathrm{III}}_B}{A^{\mathrm{III}}_B}\right)^2 + 2(c^{\mathrm{III}}_0)^2\left(\sqrt{\frac{A^{\mathrm{III}}_B}{A^{\mathrm{III}}_0}} - 1\right), \tag{160}$$

where we divided by ρ and used the definition of $c^v_0 = \sqrt{G^v_0/(2\rho)}$, $\bar{v} = Q/A$, and $p = P_{\mathrm{ext}} + G_0\left(\sqrt{A/A_0} - 1\right)$. The external pressure P_{ext} appears on both sides and therefore cancels. Finally, we can express our unknown at the bifurcation in terms of the characteristic variables $\boldsymbol{W} = (W_1, W_2)^T$, which yields three equations

$$Q^v_B = A^v_B\left(\frac{W^v_{2,B} - W^v_{1,B}}{2}\right), \quad v \in \{\mathrm{I}, \mathrm{II}, \mathrm{III}\}. \tag{161}$$

But how do we find $W^v_{2,B}$ and $W^v_{1,B}$? Here, we take an upwind decision. In the feeding vessel waves associated with W_2 travel towards the bifurcation. In the downstream vessels waves associated with W_1 travel towards the bifurcation. Therefore,

$$W^{\mathrm{I}}_{2,B} = W_2(A_K, Q_K) = \frac{Q_K}{A_K} + 4c_1(A_K), \tag{162}$$

$$W^{\mathrm{II}}_{1,B} = W_1(A_L, Q_L) = -\frac{Q_L}{A_L} + 4c_1(A_L), \tag{163}$$

$$W^{\mathrm{III}}_{1,B} = W_1(A_M, Q_M) = -\frac{Q_M}{A_M} + 4c_1(A_M). \tag{164}$$

For the complementary characteristic variables for which associated waves travel in the opposite direction, we take the information of the bifurcation, that is

$$W^{\mathrm{I}}_{1,B} = W_1(A^{\mathrm{I}}_B, Q^{\mathrm{I}}_B) = -\frac{Q^{\mathrm{I}}_B}{A^{\mathrm{I}}_B} + 4c_1(A^{\mathrm{I}}_B), \tag{165}$$

$$W^{\mathrm{II}}_{2,B} = W_2(A^{\mathrm{II}}_B, Q^{\mathrm{II}}_B) = \frac{Q^{\mathrm{II}}_B}{A^{\mathrm{II}}_B} + 4c_1(A^{\mathrm{II}}_B), \tag{166}$$

$$W^{\mathrm{III}}_{2,B} = W_2(A^{\mathrm{III}}_B, Q^{\mathrm{III}}_B) = \frac{Q^{\mathrm{III}}_B}{A^{\mathrm{I}}_B} + 4c_1(A^{\mathrm{III}}_B). \tag{167}$$

Hence after applying the upwind scheme, we have expressions for all $W^v_{2,B}$ and $W^v_{1,B}$ in terms of our unknown at the bifurcation and known values in the adjacent elements. In summary, Eqs. (158) to (161) are six (nonlinear) equations which we can solve for the six unknowns, A^{I}_B, A^{II}_B, A^{III}_B, Q^{I}_B, Q^{II}_B, Q^{III}_B.

Since the system of equations is nonlinear, we need a nonlinear solver like the Newton method. To this end, the equation can be written in residual form $\boldsymbol{R}(\boldsymbol{U}^v_B) = \boldsymbol{0}$, with the residual vector $\boldsymbol{R} \in \mathbb{R}^6$. Applying Newton's method yields the iteration rule for iteration $m+1$,

$$[\boldsymbol{U}^v_B]^{m+1} = [\boldsymbol{U}^v_B]^m - \left(\boldsymbol{J}_{\boldsymbol{R}}\left([\boldsymbol{U}^v_B]^m\right)\right)^{-1}\boldsymbol{R}\left([\boldsymbol{U}^v_B]^m\right), \tag{168}$$

where $\boldsymbol{J}_{\boldsymbol{R}} := \frac{\partial \boldsymbol{R}}{\partial \boldsymbol{U}}$ is the Jacobian matrix of the residual. In the first iteration, $[\boldsymbol{U}^v_B]^0$ is to be specified (initial guess). Ideally, the initial guess is close to the actual solution. We can start with the element values in the elements adjacent to the bifurcation which should be quite close to what we want to estimate for the bifurcation.

References

[1] Milton Abramowitz and Irene A Stegun. *Handbook of mathematical functions with formulas, graphs, and mathematical tables*, volume 55. US Government printing office, 1964.

[2] Laurence T. Baxter and Rakesh K. Jain. Transport of fluid and macromolecules in tumors. I. Role of interstitial pressure and convection. *Microvascular Research*, 37(1):77–104, 1989. doi:10.1016/0026-2862(89)90074-5.

[3] Luca Formaggia, Daniele Lamponi, and Alfio Quarteroni. One-dimensional models for blood flow in arteries. *Journal of Engineering Mathematics*, 47(3):251–276, 2003. ISSN 1573-2703. doi:10.1023/B:ENGI.0000007980.01347.29.

[4] Sergei K. Godunov and I. Bohachevsky. Finite difference method for numerical computation of discontinuous solutions of the equations of fluid dynamics. *Matematičeskij sbornik*, 47(89)(3):271–306, 1959. URL `https://hal.science/hal-01620642`.

[5] Ami Harten. High resolution schemes for hyperbolic conservation laws. *Journal of Computational Physics*, 49(3):357–393, 1983. doi:10.1016/0021-9991(83)90136-5. URL `https://doi.org/10.1016/0021-9991(83)90136-5`.

[6] Fridtjov Irgens. *Generalized Newtonian Fluids*, pages 113–124. Springer International Publishing, Cham, 2014. ISBN 978-3-319-01053-3. doi:10.1007/978-3-319-01053-3_6.

[7] Rakesh K. Jain. Transport of molecules across tumor vasculature. *Cancer and Metastasis Review*, 6(4): 559–593, 1987. doi:10.1007/bf00047468.

[8] Rakesh K. Jain, Ricky T. Tong, and Lance L. Munn. Effect of vascular normalization by antiangiogenic therapy on interstitial hypertension, peritumor edema, and lymphatic metastasis: Insights from a mathematical model. *Cancer Research*, 67(6):2729–2735, 2007. doi:10.1158/0008-5472.can-06-4102.

[9] Timo Koch. Mixed-dimension models for flow and transport processes in porous media with embedded tubular network systems, 2020.

[10] Levick. Capillary filtration-absorption balance reconsidered in light of dynamic extravascular factors. *Experimental Physiology*, 76(6):825–857, 1991. doi:10.1113/expphysiol.1991.sp003549.

[11] Vuk Milišić and Alfio Quarteroni. Analysis of lumped parameter models for blood flow simulations and their relation with 1d models. *ESAIM: Mathematical Modelling and Numerical Analysis*, 38(4):613–632, 2004. doi:10.1051/m2an:2004036.

[12] A R Pries, T W Secomb, P Gaehtgens, and J F Gross. Blood flow in microvascular networks. experiments and simulation. *Circulation Research*, 67(4):826–834, 1990. doi:10.1161/01.res.67.4.826.

[13] A. R. Pries, D. Neuhaus, and P. Gaehtgens. Blood viscosity in tube flow: dependence on diameter and hematocrit. *American Journal of Physiology-Heart and Circulatory Physiology*, 263(6):H1770–H1778, 1992. doi:10.1152/ajpheart.1992.263.6.h1770.

[14] A R Pries, T W Secomb, T Gessner, M B Sperandio, J F Gross, and P Gaehtgens. Resistance to blood flow in microvessels in vivo. *Circulation Research*, 75(5):904–915, 1994. doi:10.1161/01.res.75.5.904.

[15] Axel R Pries and Timothy W Secomb. Blood flow in microvascular networks. In *Microcirculation*, pages 3–36. Elsevier, 2008. doi:10.1016/b978-0-12-374530-9.00001-2.

[16] Alfio Quarteroni and Luca Formaggia. Mathematical modelling and numerical simulation of the cardiovascular system. In *Computational Models for the Human Body*, volume 12 of *Handbook of Numerical Analysis*, pages 3–127. Elsevier, 2004. doi:10.1016/S1570-8659(03)12001-7.

[17] Ernest H. Starling. On the absorption of fluids from the connective tissue spaces. *The Journal of Physiology*, 19(4):312–326, 1896. doi:10.1113/jphysiol.1896.sp000596.

[18] P. K. Sweby. High resolution schemes using flux limiters for hyperbolic conservation laws. *SIAM Journal on Numerical Analysis*, 21(5):995–1011, 1984. doi:10.1137/0721062.

[19] John R. Womersley. Method for the calculation of velocity, rate of flow and viscous drag in arteries when the pressure gradient is known. *The Journal of Physiology*, 127(3):553–563, 1955. doi:10.1113/jphysiol.1955.sp005276.

[20] John R. Womersley. *An Elastic Tube Theory of Pulse Transmission and Oscillatory Flow in Mammalian Arteries*. Aerospace Research Labs Wright-Patterson AFB, Ohio, United States of America, 1957. URL `https://apps.dtic.mil/sti/citations/ADB295267`.

[21] Sunčica Čanić and Eun Heui Kim. Mathematical analysis of the quasilinear effects in a hyperbolic model blood flow through compliant axi-symmetric vessels. *Mathematical Methods in the Applied Sciences*, 26 (14):1161–1186, 2003. doi:10.1002/mma.407.